P. Dagaut[1*], F. Karsenty[1], G. Dayma[1], P. Diévart[1], K. Hadj-Ali[1], A. Mzé-Ahmed[1], M. Braun-Unkhoff[2*], J. Herzler[2], T. Kathrotia[2], T. Kick[2], C. Naumann[2], U. Riedel[2], L. Thomas[2]

Experimental and detailed kinetic model for the oxidation of a Gas to Liquid (GtL) jet fuel

[1] Centre National de la Recherche Scientifique, 1C, Avenue de la Recherche Scientifique - 45071 Orléans Cedex 2 – France
[2] Institute of Combustion Technology, German Aerospace Center (DLR), Pfaffenwaldring 38-40, 70569 Stuttgart, Germany

# Experimental and Detailed Kinetic Model for the Oxidation of a Gas to Liquid (GtL) Jet Fuel

Philippe Dagaut, Florent Karsenty, Guillaume Dayma, Pascal Diévart, Kamal Hadj-Ali, Amir Mzé-Ahmed,

*Centre National de la Recherche Scientifique, 1C, Avenue de la Recherche Scientifique - 45071 Orléans Cedex 2 – France*


Marina Braun-Unkhoff, Jürgen Herzler, Trupti Kathrotia, Thomas Kick, Clemens Naumann, Uwe Riedel, Levi Thomas†

*Institute of Combustion Technology, German Aerospace Center (DLR), Pfaffenwaldring 38-40, 70569 Stuttgart, Germany*

*†On exchange from Wright Patterson Air Force Base – Ohio, USA*


Correspondence:

Philippe Dagaut

Email: dagaut@cnrs-orleans.fr

Tel.: +33 238 255466          Fax: +33 238 696004

Marina Braun-Unkhoff

Email: Marina.Braun-Unkhoff@dlr.de

Tel. +49 7116862508          Fax +49 7116862578

Shortened running title: GTL Jet Fuel Oxidation

**ABSTRACT**

The kinetics of oxidation, ignition, and combustion of Gas-to-Liquid (GtL) Fischer-Tropsch Synthetic kerosene as well as of a selected GtL-surrogate were studied. New experimental results were obtained using (i) a jet-stirred reactor – species profiles (10 bar, constant mean residence time of 1 s, temperature range 550-1150 K, equivalence ratios $\varphi$ = 0.5, 1, and 2), (ii) a shock tube – ignition delay time ($\approx$ 16 bar, temperature range 650-1400 K, $\varphi$ = 0.5 and 1), and (iii) a burner - laminar burning velocity (atmospheric pressure, preheating temperature = 473 K, $1.0 \leq \varphi \leq 1.5$). The concentrations of the reactants, stable intermediates, and final products were measured as a function of temperature in the jet-stirred reactor (JSR) using probe sampling followed by on-line Fourier Transformed Infra-Red spectrometry, and gas chromatography analyses (on-line and off-line). Ignition delay times behind reflected shock waves were determined by measuring time-dependent CH* emission at 431 nm. Laminar flame speeds were obtained in a bunsen-type burner by applying the cone angle method. Comparison with the corresponding results for Jet A-1 showed comparable combustion properties. The GtL-fuel oxidation was modeled under these conditions using a detailed chemical kinetic reaction mechanism (8217 reactions *vs*. 2185 species) and a 3-component model fuel mixture composed of *n*-decane, *iso*-octane (2,2,4-trimethyl pentane), and *n*-propylcyclohexane. The model showed good agreement with concentration profiles obtained in a JSR at 10 bar. In the high temperature regime, the model represents well the ignition delay times for the fuel air mixtures investigated; however, the calculated delays are longer than the measurements. It was observed that the ignition behavior of the surrogate fuel is mainly influenced by *n*-alkanes and not by the addition of *iso*-alkanes and *cyclo*-alkanes. The simulated laminar burning velocities were found in excellent agreement with the measurements. No deviation between burning velocity data for the GtL-surrogate and GtL was seen, within the uncertainty range. The presented data on ignition delay times and

burning velocities agree with earlier results obtained for petrol-derived jet fuel. The suitability of both the current detailed reaction model and the selected GtL surrogate was demonstrated. Finally, our results support the use of the GtL fuel as an alternative jet fuel.

## 1. INTRODUCTION

Fossil fuels are currently the primary energy source worldwide [1]. In the 21st century, alternative energy resources became increasingly used [2] to guarantee security of supply and to mitigate global warming. Correspondingly, the search for alternative aviation fuels has grown rapidly over the last 10 years. In 2011, the European Advanced Biofuels Flight Path was launched by the European Commission for the purpose of accelerating the commercialization of aviation biofuels [3]. However, this effort is technically challenging due to strict fuel specifications which include: fuel freezing point, energy density, flash point, flammability limit, and amount of aromatics [4, 5]. It is important, therefore, to improve our knowledge of synthetic jet fuel properties through experimental characterization and computational fluid dynamics modeling. For optimizing applications of synthetic fuels in aero-engines, their combustion properties must be well characterized and understood. Therefore, ignition delay times and laminar flame speed as well as transient chemical species and combustion products, must be measured over a broad range of conditions (temperature, pressure, fuel composition, and equivalence ratio). Nevertheless, only limited data sets exist for the combustion of synthetic jet fuels which are complex mixtures of several chemical classes [6, 7].

Measurement of the ignition delay time of kerosene [7-12] and of GtL [8, 10-12], has been the subject of a few studies while some data exist for various surrogates [7, 9, 13-16]. Concerning laminar flame speed measurements of GtL fuels, only a few investigations are published [17-20].

Concerning modeling the oxidation of a jet fuel, it is not possible to incorporate in the reaction model all of the species composing kerosene. Instead, a surrogate is used, with a limited number of compounds with known kinetic sub-models as a means to represent kerosene [4]. Surrogates should show a behavior similar to that of commercial jet fuels, ideally for predicting both chemical and physical properties. Such surrogates are of high interest since they can be utilized to study the effect of chemical composition and fuel properties on the combustion process. Depending on the objective, 3-7 well-selected hydrocarbons might be present in the initial formula of a surrogate, to describe the combustion properties of practical blends. Presently, many proposals concerning the composition of a surrogate fuels exist, see *e.g.* [4, 7, 9, 14, 15].

As part of continuing efforts in our laboratories to improve our knowledge of fuels combustion, the oxidation kinetics of a GtL jet fuel and a selected GtL surrogate were studied in a jet-stirred reactor (JSR) at 10 bar, over a range of temperatures and equivalence ratios. Ignition delays of GtL/synthetic air mixtures diluted in nitrogen and of a GtL-surrogate blend were measured. The experiments were performed at initial pressures of about 16 bar and at two equivalence ratios. Burning velocities of the GtL jet fuel and of a selected surrogate mixed with air were measured at ambient pressures and a preheating temperature of 473 K. A detailed chemical kinetic reaction mechanism was proposed to represent the present data, complementing recent developments on the formulation of alternative jet fuel surrogates and kinetic combustion models [8, 9, 21].

## 2. EXPERIMENTAL

To understand a fuel's combustion under aero-turbine operating conditions several aspects have to be considered. These processes occur over a range of temperatures, pressures, and fuel-air ratios and are considered to be among the most important operating parameters for an

aero-turbine. The main focus of the current work is the oxidation of the fuel and the formation of pollutants but also major combustion properties, i.e. burning velocity and ignition. To investigate each of these parameters, complementary experimental systems were used: a jet stirred reactor for studying fuel oxidation and pollutants formation, a shock tube to study self-ignition of the fuel, and a flame test rig to measure laminar flame speeds. Each test rig was used to investigate the combustion of several fuels; the results were used for developing a detailed kinetic reaction scheme. The same GtL fuel was used in all the experiments (JSR, shock tube, and flame): a GtL Fischer-Tropsch synthetic jet fuel provided by Shell ($C_{10.45}H_{23.06}$, M=148.44 g·mol$^{-1}$, density=737.7 g·l$^{-1}$, composition in mass %: 28.1% *n*-alkanes, 62.8% *iso*-alkanes, 8.8% *cyclo*-alkanes, and 0.2% aromatics). Detailed GC/MS analyses were used to determine the mass composition of the fuel and derive the global chemical formula used here (see Section 3).

## 2.1 Jet stirred reactor

The experiments were performed in the JSR set-up used previously [22-24]. It consists of a 39 cm$^3$ fused-silica sphere to avoid wall catalyzed reactions. The reactor has four injectors with nozzles of 1 mm inner diameter (ID) which both admit and stir the gases. A 100 l·h$^{-1}$ nitrogen flow was used to dilute the fuel. As presented before [23, 24], all gases were preheated to a temperature close to that in the JSR prior to injection in order to reduce temperature gradients. The selected operating temperatures in the reactor were maintained thanks to a regulated oven. The reactants were mixed just before reaching the injectors. Nitrogen (<50 ppm of $O_2$; <1000 ppm of Ar; <5 ppm of $H_2$, Air Liquide) was used as bath gas and oxygen (99.995% pure, Air Liquide) was the oxidizer. The gases were delivered by mass flow meters (Brooks 5850E and 5850TR). A HPLC pump with on-line degasser (Shimadzu) was used to convey the fuel to a temperature-controlled atomizer-vaporizer assembly (523 K).

For each experiment a Pt-Pt/Rh 10% thermocouple (0.1 mm ID) located inside a thin-wall silica tube was used to verify thermal homogeneity all along the vertical axis of the reactor. The reacting mixtures were probe sampled by a fused-silica low-pressure sonic probe (~4-6 kPa). The samples were collected at steady residence time and temperature. They were analyzed on-line by gas chromatography-mass spectrometry (GC-MS Saturn 2000, Varian) and Fourier Transformed Infra-Red spectrometry (FTIR Nicolet Magna 550; 2 m path length, 1 cm$^{-1}$ resolution), and off-line, after storage in 1 l Pyrex bulbs, by GC. Permanent gases and light compounds were analyzed off-line whereas high boiling point compounds were analyzed on-line by GC. The experiments were performed at steady state and at a constant mean residence time with the reactants constantly flowing into the reactor while the temperature of the reacting gases was varied stepwise. Highly diluted mixtures were used for preventing flame occurrence, reducing heat release, and minimizing temperature gradients (~1 K cm$^{-1}$) in the reactor. The working pressure was measured at the exhaust using a high precision gauge. GCs with capillary columns (DB-5 ms: 30 m and 0.32 mm ID, DB-624: 60 m and 0.32 mm ID, Plot $Al_2O_3$/KCl: 50 m and 0.32 mm ID, Carboplot-P7: 25 m and 0.53 mm ID), a thermal conductivity detector and a flame ionization detector were used for quantifying stable species. For compound identification we used a quadrupole mass spectrometer (GC/MS Varian 1200), operating in electron impact ionization mode (70 eV). On-line FTIR analyses were also performed allowing the quantification of $H_2O$, CO, $CO_2$, $CH_2O$, $CH_4$, and $C_2H_4$. The fused-silica sampling probe was connected to a temperature controlled (413 K) gas cell via a 6.35 mm (OD) deactivated stainless steel heated line (413 K). The present measurements showed good repeatability and good carbon balance (100±15%) was determined. Uncertainties on concentration profiles were evaluated to be less than 15%. The accuracy of temperature measurements was better than 5 K.

**2.2 Shock tube**

The experiments were carried out in a high pressure shock tube with an internal diameter of 46 mm. It is divided by aluminum diaphragms into a driver section of 10.0 m and a driven section of 3.25 m in length. The driver section is heated to 393 K. Helium was the main driver gas while argon was added to match the acoustic impedance of the shock heated driven gas. The exact mixture ratio was achieved using two mass flow meters (EL-FLOW®, Bronkhorst) with an accuracy of 0.5% of the measurement value and 0.1% of the maximum flow, respectively. These tailored conditions extended the observation period to longer measurement times [17, 25]. The driven section was heated to 433 K and pumped down to pressures below $10^{-4}$ mbar by a turbo-molecular pump. Gas mixtures were prepared manometrically in a 5 l stainless steel vessel heated to 453 K and evacuated below pressures of $10^{-4}$ mbar using a separate turbo molecular pump. For each experiment, a new mixture was prepared by injecting the fuel blend with a syringe into the evacuated vessel and mixing it with synthetic air (80/20 vol% $N_2/O_2$) and additional nitrogen for dilution. After a mixing time of 30 min the fuel/air/$N_2$ mixture was released into the shock tube. For the experimental series the mixture was controlled by gas chromatographic analyses such that all components of the mixture evaporate in the mixing vessel and the mixture remains stable during the mixing time. The time which is needed for a perfect mixing was also determined by gas chromatography. It was also confirmed that no condensation occurred in the shock tube. Pressure and temperature behind the reflected shock wave were calculated from the measured incident shock wave velocity and attenuation using a one-dimensional shock model. Thus, the incident shock speed was measured over three 200 mm intervals along the tube and over four 32 mm intervals in the vicinity of the end flange using four and five piezo-electric pressure gauges, respectively. The uncertainty in reflected shock temperature is estimated to be less than 15 K in the temperature range of our measurements.

The ignition was observed by measuring the CH* emission at 431 nm 10 mm in front of the end plate applying a narrow band pass filter (FWHM – full width half maximum = 5 nm) and a photomultiplier. In the same measurement plane, pressure profiles with piezo-electric gauges (PCB[®] 112A05 and Kistler[®] 603B) were recorded. All the ignition delay times reported here were determined by measuring the time difference between the initiation of the reaction system by the reflected shock wave and the occurrence of the maximum emission of CH*. This permits a good comparability to kinetic simulations either using a CH* sub-model or simply the CH-concentration profiles. The experimental setup in combination with the tailored interface conditions allowed measurements of ignition delay times up to 40 ms depending on the temperature.

## 2.3 Burner

The commonly known cone angle method [26] was applied for the measurement of the burning velocities of the vaporized fuels. The experimental set up (Fig. 1) consisted of a flame holder, a metering pump for liquid fuel (HPLC pump, Shimadzu, Prominence LC-20AD), a fuel evaporator (Institut für Chemische Verfahrenstechnik, Stuttgart University) [27], mass flow meters (MFC, Bronkhorst) to adjust nitrogen and oxygen flows, and the mixing section. The oxygen dissolved in the liquid fuel was displaced by helium sparkling. After evaporation at temperatures up to about 580 K, the fuel was added to the preheated nitrogen flow. As demonstrated by Edwards and Atria [28], cracking and thermal degradation of deoxygenated fuels is negligible at 580 K. After the fuel addition, the fuel-nitrogen mixture was cooled to 480 K before the mixture was combined with the oxygen flow to avoid premature ignition. Afterwards the gaseous flows were homogenized. The ratio of oxygen to nitrogen flow was set to 21:79 mol% percent for emulating fuel-air composition. The sections conducting

oxygen-nitrogen fuel mixtures were heated to 480 K. The desired temperature of the unburned air-fuel mixture was achieved by controlling the temperature of the flame holder.

Cone-shaped flames were stabilized on the flame holder's nozzle. Flames with variable equivalence ratios were achieved by using nozzles with different diameters. Images of the flames were recorded by an electronic camera (La Vision, Imager Pro Plus 2M, 1200x1600 pixel). The images were treated by a low pass filter, after which contours were resolved by determining the two picture elements with the highest brightness values in each line. Selected parts of the contours were then used to calculate the cone angles $\alpha$. Values of $S_u$ were given by the cone angles $\alpha$ and the velocities $v_u$ of the unburned gas, whereas $v_u$ was derived from the volumetric flow rate and the nozzle diameter:

$$S_u = v_u \sin \alpha \quad (1).$$

At equivalence ratios from $\varphi \sim 1.0$ up to $\varphi = 1.5$ conical flames were stabilized. Decreasing the equivalence ratio from $\varphi \leq 1.0$, the cone-shaped flames suited for determination of $S_u$ could not be stabilized. At increasing equivalence ratios $\varphi \geq 1.45$, the fluctuations in the flame contour increased resulting in a larger variance of $S_u$ values. At equivalence ratios $\varphi > 1.5$ either the contour became wrinkled [17], or the flame tip opened, making accurate measurement of burning velocity impossible.

The accuracy of the burning velocity determination is affected by error in the following experimental parameters: mass flow and temperature of unburned gas mixture, pressure, orifice area of the nozzles, and determination of cone angle. The inaccuracies of each one of these parameters were in the order of 1 to 1.5%, leading to a total error of up to 5% of the measured burning velocity. The maximum error of the determination of the equivalence ratio of ± 2% is due to deviations of the actual fuel/oxygen flow ratios from specified values.

In addition, possible methodical errors of the applied technique should also be considered. First, flame strain and curvature [29]; furthermore, a deviation of the flow pattern from the

ideal plug flow [30] might occur. In the literature [31], a comparison of laminar flame speeds determined by different techniques is discussed. Wu and Law considered nozzle burners with conical and button shaped flames, spherical flames in closed vessel combustors, and counter flow burners. They also pointed out the effect of the heat conductivity and diffusivities of the components of the gas mixtures on the burning velocity of stretched flames. For these reasons, burning velocities measured in the present work may differ from those obtained by more exact stretch corrected methods. In general, the stretch rate $K$ (s$^{-1}$) of a premixed flame is given by:

$$K = \frac{1}{A} \cdot \frac{dA}{dt} , \qquad (2)$$

$A$: unit area of the flame front.

In the case of conical flames, $K$ can be written as:

$$K = \frac{-v_u \cdot \sin(2\alpha)}{2r} \qquad (3) \quad .$$

Markstein [32] formulated a relationship between $K$ and $S_u$, the stretched burning velocity:

$$S_u = S_n - K \cdot L , \qquad (4)$$

where:

$$L = Ma \cdot \delta \qquad (5)$$

$$\delta = \frac{v}{S_n} . \qquad (6)$$

$S_n$: unstretched burning velocity,

$r$: relevant radius of conical flames,

$L$: Markstein length,

$Ma$: Markstein number,

$\delta$: thickness of flame front,

$v$: kinematic viscosity of the unburned gas [18].

Values of *Ma* for air mixtures of Jet A-1 and of GtL, respectively were determined recently by Vukadinovic *et al.* [18] applying spherical expanding flames, in the $\varphi$ range from 0.7 to 1.4. On the basis of these values, the burning velocities reported in the present work may differ from stretched corrected values: up to -10% lower in the fuel rich regime ($\varphi = 1.5$) and up to + 5% higher at stoichiometric conditions.


**3. MODELING**

The kinetic modeling was performed using the CHEMKIN II package [33, 34]. The PSR computer code [35] was used to compute species concentrations under isothermal conditions. The reaction rates were computed from the kinetic reaction mechanism and the rate constants calculated at the experimental temperature. The modified Arrhenius equation, $k = A\,T^b\,\exp(-E/RT)$ was used. The reverse reactions rate constants were computed from the corresponding equilibrium constants, $K_c = k_{forward} / k_{reverse}$, calculated from thermochemistry [36] and the forward rate constants.

The shock tube kinetic modeling was carried out using a Multiple Plug Flow Reactor (MPFR) code developed at DLR Stuttgart to take into account gas dynamic effects which cause pressure and temperature variations; for details see [21]. The MPFR code which is an extension to SENKIN based on the CHEMKIN II package [34, 37] decouples the effects of heat release and combines pressure relaxation effects along the shock propagation direction. For a short time period depending on the heat release ($\Delta T/T \leq 0.5\%$), the calculation assumes a PFR model with constant pressure conditions to take into account the pressure increase by heat release within the chosen PFR time step. The correction of the gas dynamic effects is based on pressure profiles obtained from experiments with non-reactive mixtures, with no heat release from chemical reactions; but with similar acoustic properties than the fuel to be investigated. For the simulation of the measured profiles with detailed reaction models, the

temperature profiles calculated under the assumption of adiabatic and isentropic conditions are used, instead of constant initial temperatures temperature after the reflected shock wave. A typical experimental pressure profile, clearly demonstrating the absence of any ignition during the observation period, is given in Fig. 2 together with the calculated temperature profile. The pressure profile shown is identical to experiments with no reactive mixture (air) as test gas; consequently, no heat release of the mixture is occurring.

Laminar flame speeds were calculated by using PREMIX [38] assuming a freely propagating one-dimensional flame, including thermal diffusion. In general, more than 100 mesh points were calculated, in order to ensure no further evolution in the laminar flame speed values.

One major goal of the present study is the development of a detailed chemical kinetic reaction model capable to describe the combustion and ignition of a GtL jet fuel, within a wide parameter range (temperature, pressure, and fuel-air mixture), based on relevant experimental investigations applying the three different methods described earlier. It is desirable to achieve a *single* reaction model which succeeds in describing correctly the three different kinds of experimental data (species profiles, ignition delay time, and burning velocity), within the parameter range considered. Such a model would offer the advantages of reduced time and cost expenses required for experimentation and, furthermore, would enable numerical calculations, with the interaction between turbulence and chemical kinetics taken into account.

The detailed chemical kinetic reaction mechanism of the present work is based on previous modeling efforts for describing the oxidation of conventional and synthetic jet fuels with simple surrogates [36]. It includes both low- and high-temperature reactions for the surrogate fuel components (*n*-decane, *iso*-octane, and *n*-propylcyclohexane). High temperature reaction classes include unimolecular fuel decomposition, H-atom abstraction

12

from the fuel, hydrocarbon radical decomposition, hydrocarbon radical summarization, alkene decomposition, H-atom abstraction reactions from alkenes, addition of O and OH to alkenes, alkoxy decomposition, reactions of alkenyl radicals with $HO_2$, alkenyl radical decomposition, and retro-ene decomposition reactions. Low-temperature reaction classes include addition of $O_2$ to hydrocarbon radicals forming peroxy radicals (R + $O_2$ = ROO) and their chemistry (isomerization to QOOH and subsequent reactions, i.e., QOOH = cyclic ether + OH, QOOH = alkene + $HO_2$, QOOH = alkene + carbonyl + OH, QOOH + $O_2$ = OOQOOH, OOQOOH = OQ'OOH + OH, OQ'OOH = OQ'O + OH). Other peroxy reactions were included, i.e., ROO + R = RO + RO, ROO = alkene + $HO_2$, ROO + $HO_2$ = ROOH + OH, ROO + $H_2O_2$ = ROOH + $HO_2$, ROO + ROO = RO + RO + $O_2$, and ROOH = RO + OH. The resulting detailed chemical kinetic reaction mechanism consisting of 8217 reactions involving 2185 species is available from the authors.

The surrogate is formulated in accordance to the chemical composition of the fuel determined via GC analyses; representative hydrocarbons were chosen, in line with earlier work on jet fuels combustion [21, 36]. Accordingly, in the calculations, the fuel was represented by a mixture of *n*-decane, *iso*-octane, and *n*-propylcyclohexane. To represent 1000 ppm of fuel, the following mole fractions for the model fuel #1 were used: *n*-$C_{10}H_{22}$: 0.000652, *iso*-$C_8H_{18}$: 0.000375, *n*-propylcyclohexane: 0.000103, and for the model fuel #2: *n*-$C_{10}H_{22}$: 0.000730, *iso*-$C_8H_{18}$: 0.000224, *n*-propylcyclohexane: 0.000091. Relative properties of the model fuels and the GtL jet fuel are compiled in Table 1. One should note that because the surrogates are lighter than the GtL fuel, 11 to 13% more surrogate is needed to match the carbon content in the GtL. This approximation has been used previously for representing other jet fuels [4].

Table 1. Fuels properties selected

| Property | GtL fuel | Model fuel #1 | Model fuel #2 |
|---|---|---|---|
| Formula | $C_{10.45}H_{23.06}$ | $C_{10.45}H_{22.95}$* | $C_{10.45}H_{22.92}$‡ |
| H/C | 2.2067 | 2.1966 | 2.1933 |
| Molar weight (g·mol$^{-1}$) | 148.44 | 148.31* | 148.32‡ |
| Density (g·l$^{-1}$) at 15°C | 737.7 | 723 | 725 |
| Derived Cetane Number† | 58.0 | 54.5 | 58.2 |

* 1.13 × $C_{9.2451}H_{20.308}$ since we used 1130 ppm of model fuel to represent 1000 ppm of GtL.
‡ 1.111 × $C_{9.405}H_{20.628}$ since we used 1111 ppm of model fuel to represent 1000 ppm of GtL.
† Derived Cetane Number (ASTM D7668) measured using a Herzog Cetane ID 510.

The same composition was used in all the computations presented here. The model fuel composition was chosen on the basis of GC and GC/MS multidimensional analyses (62.8% iso-alkanes − mainly $C_{10}$ to $C_{12}$, 28.1% n-alkanes − mainly $C_9$ to $C_{11}$, 0.6% mono-naphthenes − mainly $C_9$ to $C_{11}$, 8.2% di-naphthenes − mainly $C_{10}$ to $C_{11}$, 0.2% mono-aromatics − mainly $C_9$ to $C_{10}$, all in mass %) and previous studies on SPK (synthetic paraffinic kerosene) and SPK/Jet A-1 oxidation [36]. Iso-octane is more branched than the iso-alkanes present in the GtL fuel (principally mono-methyl alkanes); hence, less iso-octane is needed to represent the iso-alkane fraction of the fuel [36]. To address properly this parameter, the fraction of n-alkanes must be increased significantly while reducing that of iso-alkanes. Thus, the model fuel's composition mimics the GtL with respect to paraffins (91% in both fuels) and naphthenes (8.75% in the model fuel vs. 8.8% in the GtL), respectively.

## 4. RESULTS AND DISCUSSION

### 4.1 Oxidation in JSR

1000 ppm of GtL were oxidized in a JSR at 10 bar, at a mean residence time of 1 s, over the temperature range of 550 to 1150 K, and at three equivalence ratios $\varphi$ = 0.5, 1.0, and 2.0 (Figs. 3-5). Under these conditions, the fuel oxidized rapidly, yielding saturated (mostly methane) and unsaturated (olefins) hydrocarbon intermediates, and oxygenates (mainly formaldehyde and carbon monoxide). Over the temperature range 550-730 K, a cool flame was observed. We measured mole fractions of the reactants, main stable intermediates, and products (i.e., oxygen, hydrogen, water, carbon monoxide, carbon dioxide, formaldehyde, methane, ethane, ethylene, acetylene, propane, propene, 1-butene, 2-butenes, isobutene, 1,3-butadiene, isoprene, 1,3-pentadiene, benzene, and cyclohexene) as a function of temperature;. A good repeatability of the results was observed. The accuracy of the mole fractions, derived from repeated experiments and repeated analyses, was typically ±10% and better than 15% whereas the uncertainty on the experimental temperature was ±5 K. It can be seen from Table 2, that reports the maximum mole fractions of measured species, that the main products were $CO_2$, CO, $H_2O$, $CH_2O$, $CH_4$, $C_2H_4$, and $C_3H_6$. Their mole fractions were larger under the high-temperature oxidation regime than under cool-flame conditions.

Table 2. Measured products during the oxidation of the stoichiometric GtL/oxygen/nitrogen mixture in a JSR at 10 bar.

| Measured Products | Maximum Mole Fraction | |
|---|---|---|
| | at low temperature | at high temperature |
| $H_2O$ | $2.3 \times 10^{-3}$ | $8.8 \times 10^{-3}$ |
| $CO_2$ | $3.4 \times 10^{-4}$ | $8.2 \times 10^{-3}$ |
| $H_2$ | $1.3 \times 10^{-5}$ | $4.3 \times 10^{-4}$ |
| CO | $1.3 \times 10^{-3}$ | $5.9 \times 10^{-3}$ |
| $CH_2O$ | $3.1 \times 10^{-4}$ | $3.1 \times 10^{-4}$ |

| | | |
|---|---|---|
| $CH_4$ | * | $4.0 \times 10^{-4}$ |
| $C_2H_6$ | * | $3.0 \times 10^{-5}$ |
| $C_2H_4$ | * | $9.9 \times 10^{-4}$ |
| $C_3H_6$ | * | $2.4 \times 10^{-4}$ |
| $1\text{-}C_4H_8$ | * | $5.2 \times 10^{-5}$ |
| $1\text{-}C_5H_{10}$ | * | $2.3 \times 10^{-5}$ |
| $1\text{-}C_6H_{12}$ | * | $1.8 \times 10^{-5}$ |
| *trans*-2-$C_4H_8$ | * | $6.5 \times 10^{-6}$ |
| *cis*-2-$C_4H_8$ | * | $4.7 \times 10^{-6}$ |
| *trans*-2-$C_5H_{10}$ | * | $1.4 \times 10^{-6}$ |
| *cis*-2-$C_5H_{10}$ | * | $6.0 \times 10^{-6}$ |
| *iso*-$C_4H_8$ | * | $2.2 \times 10^{-5}$ |
| isoprene | * | $4.2 \times 10^{-6}$ |
| $C_2H_2$ | * | $1.1 \times 10^{-5}$ |
| $1,3\text{-}C_4H_6$ | * | $1.7 \times 10^{-5}$ |
| $1,3\text{-}C_5H_8$ | * | $4.6 \times 10^{-6}$ |
| *cyclo*-$C_5H_8$ | * | $4.4 \times 10^{-6}$ |
| *cyclo* $C_6H_{10}$ | * | $1.3 \times 10^{-6}$ |

* Maximum not detected

The experimental results were compared to previously obtained data for the oxidation of a typical Jet A-1. As can be seen from Fig. 6a, the two fuels oxidize similarly. However, it was observed that under cool flame conditions (550-750 K) the oxidation of Jet A-1 is faster than GtL, leading to larger formation of stable intermediates ($CH_2O$ and CO) and products ($H_2O$ and $CO_2$). At higher temperature both fuels seem to oxidize at the same rate. But, some interesting differences appear for intermediate hydrocarbons. The oxidation of Jet A-1 yields

significantly less methane, ethylene and propene than the GtL oxidation. These differences must be attributed to the larger fractions of paraffins in the GtL that produce simple olefins by β-scission whereas methane enhanced production reflects the higher *iso*-alkane content in the GtL. Figure 6b compares the present data with those obtained with a CtL [21]. Again, differences in terms of reactivity and formation of intermediates must be attributed to strong composition differences. The small concentration of n-alkanes in the CtL yields lower low-temperature reactivity and lower ethylene production.

In Figs. 3-5, the concentrations of the most important intermediates and products (see Table 2) are reported. The proposed kinetic model (model fuel#1) represents the data fairly well, even under cool flame conditions where the model tends to under-predict the formation of CO, $CO_2$, and $H_2O$ whereas that of formaldehyde is over-predicted. That could be explained by underestimation of chain branching processes such as the decomposition of ketohydroperoxides. At higher temperatures, the intermediate formation of ethylene is increasingly underestimated when the equivalence ratio increases. This trend is less significant here than for other models, as shown in a recent study of n-undecane oxidation under similar conditions [39]. One can see potential for improvements exists. They should be attainable by using a more complex composition of the model fuel which would however irremediably increase the size and complexity of the kinetic reaction mechanism. Also, a variation of the composition of the model fuel could help improve the computation. To this end, a second model fuel was used. Its composition differs moderately from that of the model fuel #1, but its cetane number better matches that of the GtL (Table 1). As can be seen from Figs. 7-9 little modeling improvements were obtained with the model fuel #2 under fuel-lean conditions whereas the modeling gets worse at higher equivalence ratios. Therefore, we used only the model fuel #1 in the rest of the study.
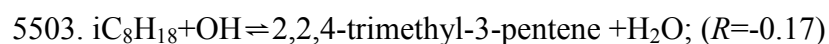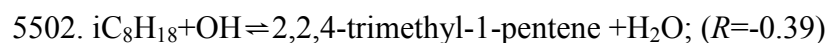
Before proceeding further, we tested the validity of the kinetic scheme against new data obtained for the oxidation of a fuel having the exact composition of the model fuel (in mole fractions, $n$-$C_{10}H_{22}$: 0.000652, $iso$-$C_8H_{18}$: 0.000375, $n$-propylcyclohexane: 0.000103). As can be seen from Fig. 10, the proposed model represents very well this additional set of data.

Reaction flux analyses showed that the model fuel#1's components are primarily oxidized by H-abstraction with OH radicals ($\varphi = 1.0$, 900 K, 1 s).

*n-decane:*

1914. $n$-$C_{10}H_{22}$+OH$\rightleftharpoons$$H_2O$+1-$C_{10}H_{21}$; ($R$=-0.11)

1915. $n$-$C_{10}H_{22}$+OH$\rightleftharpoons$$H_2O$+2-$C_{10}H_{21}$; ($R$=-0.20)

1916. $n$-$C_{10}H_{22}$+OH$\rightleftharpoons$$H_2O$+3-$C_{10}H_{21}$; ($R$=-0.20)

1917. $n$-$C_{10}H_{22}$+OH$\rightleftharpoons$$H_2O$+4-$C_{10}H_{21}$; ($R$=-0.20)

1918. $n$-$C_{10}H_{22}$+OH$\rightleftharpoons$$H_2O$+5-$C_{10}H_{21}$; ($R$=-0.20)

*Iso-octane*:

5502. $iC_8H_{18}$+OH$\rightleftharpoons$2,2,4-trimethyl-1-pentene +$H_2O$; ($R$=-0.39)

5503. $iC_8H_{18}$+OH$\rightleftharpoons$2,2,4-trimethyl-3-pentene +$H_2O$; ($R$=-0.17)

5504. $iC_8H_{18}$+OH$\rightleftharpoons$2,4,4-trimethyl-2-pentene +$H_2O$; ($R$=-0.13)

5505. $iC_8H_{18}$+OH$\rightleftharpoons$2,4,4-trimethyl-1-pentene +$H_2O$; ($R$=-0.14)

*n-propylcyclohexane (*pch*):*

2992. pch+OH$\rightleftharpoons$pchA ($C_6H_{11}CH_2CH_2CH_2$)+$H_2O$; ($R$=-0.11)

2993. pch+OH$\rightleftharpoons$pchB ($C_6H_{11}CH_2CHCH_3$)+$H_2O$; ($R$=-0.07)

2994. pch+OH$\rightleftharpoons$pchC ($C_6H_{11}CHCH_2CH_3$)+$H_2O$; ($R$=-0.07)

2995. pch+OH$\rightleftharpoons$pchD (1-C$_6$H$_{10}$C$_3$H$_7$)+H$_2$O; ($R$=-0.1)

2996. pch+OH$\rightleftharpoons$pchE (2-C$_6$H$_{10}$C$_3$H$_7$)+H$_2$O; ($R$=-0.2)

2997. pch+OH$\rightleftharpoons$pchF (3-C$_6$H$_{10}$C$_3$H$_7$)+H$_2$O; ($R$=-0.2)

2998. pch+OH$\rightleftharpoons$pchG (4-C$_6$H$_{10}$C$_3$H$_7$)+H$_2$O; ($R$=-0.1)

Among the main products, methane is mostly produced by methyl radicals' reactions with HO$_2$, formaldehyde, and ethylene:

75. CH$_3$+HO$_2$$\rightleftharpoons$CH$_4$+O$_2$; ($R$=0.18)

199. CH$_2$O+CH$_3$$\rightleftharpoons$HCO+CH$_4$; ($R$=0.38)

238. C$_2$H$_4$+CH$_3$$\rightleftharpoons$C$_2$H$_3$+CH$_4$; ($R$=0.09)
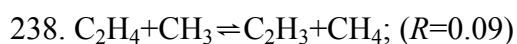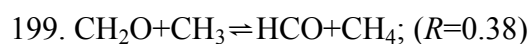
Ethyl radicals' oxidation and beta-scissions produce ethylene:

217. C$_2$H$_5$+HO$_2$$\rightleftharpoons$C$_2$H$_4$+H$_2$O$_2$; ($R$=0.03)

231. C$_2$H$_4$+HO$_2$$\rightleftharpoons$C$_2$H$_4$O$_2$H; ($R$=0.29)
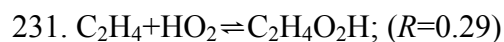
325. C$_2$H$_5$O$_2$$\rightleftharpoons$C$_2$H$_4$+HO$_2$; ($R$=0.19)

463. n-C$_3$H$_7$(+M)$\rightleftharpoons$C$_2$H$_4$+CH$_3$(+M); ($R$=0.09)

The oxidation of vinyl and hydroxymethyl radicals and the decomposition of methoxy radicals yield formaldehyde:

2. C$_2$H$_3$+O$_2$$\rightleftharpoons$CH$_2$O+HCO; ($R$=0.36)
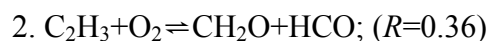
161. CH$_2$OH+O$_2$$\rightleftharpoons$CH$_2$O+HO$_2$; ($R$=0.07)

165. CH$_3$O+M$\rightleftharpoons$CH$_2$O+H+M; ($R$=0.2)

Reactions pertaining to the oxidation sub-scheme of *iso*-octane are responsible for the formation of *iso*-butene:

5395. tC$_4$H$_9$+O$_2$$\rightleftharpoons$iC$_4$H$_8$+HO$_2$; ($R$=0.4)
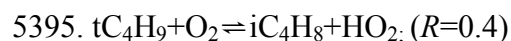
5592. 2,4,4-trimethyl-2-pentene $\rightleftharpoons tC_4H_9 + iC_4H_{8;}$ ($R$=0.3)

## 4.2 Ignition in shock tube

For all three fuel-air mixtures investigated GtL, the selected GtL surrogate, and mixtures of Jet A-1 [40] in synthetic air (20% $O_2$ / 80% $N_2$) - ignition delay time data were determined at elevated pressures around 16 bar and temperatures between 650 and 1400 K. Experiments were done for two equivalence ratios, $\varphi = 0.5$ and $\varphi = 1.0$, at a dilution of 1:2, with nitrogen. The GtL surrogate consists of *iso*-octane (33.2 mol %), *n*-decane (57.7 mol %) and *n*-propylcyclohexane (9.1 mol %). As described earlier, the CH* emission observed at 431 nm was chosen as the criteria for the occurrence of ignition, and the ignition delay time was defined as the time period between the initiation of the reactive system by the reflected shock front and the CH* maximum emission (see Fig. 11).

Computations were performed using the present kinetic reaction model enabling comparison between measured and predicted data applying the MPFR code [34, 37, 41]. The averaged pressure profile based on several experiments with non-reacting mixtures (synthetic air with nitrogen for dilution) which we used for all experiments is given in Table 3. It was not necessary to use different pressure profiles because the height of maximum and the small pressure drop after the maximum are almost identical for all used conditions of this work (see e.g. Fig. 2 and Fig. 11). The time of the maximum slightly differs with the temperature (shock speed) of the experiment but this has only a small influence on the simulations because the temperature changes in the region of the maximum are quite small (less than 15 K, see Fig. 2). The influence of the temperature increase due to gas dynamic compression is also very small for long ignition delay times because for T < 900 K the ignition delay times for stoichiometric mixtures in the NTC (negative temperature coefficient) region are almost independent on the

temperature, see Figs. 13-14. In accordance to the experiments, the same criteria (CH* maximum concentration) was chosen as the indicator for the ignition.

The comparison between the results of the measurements and the reaction model predictions for the GtL and Jet A-1 surrogate (69% *n*-decane,; 11%; *n*-propylcyclohexane, 20% *n*-propylbenzene, in mol) [42] are shown in Figs. 12-17. The measured ignition delay times for GtL, the GtL surrogate, and Jet A-1 are mostly very close to each other besides for temperatures $T < 1100$ K: at these temperatures, ignition delay times of GtL and GtL surrogate were slightly shorter when compared to those of Jet A-1. The predictions with the surrogates for kerosene and GtL also differ slightly, but do yield significantly longer ignition delay times when compared to experimental data. The temperature dependence within the NTC range is not predicted well as the simulated temperature dependence is much stronger than the experimentally observed one (Fig. 13, $\varphi = 1.0$). The experiments show almost constant ignition delay times for temperatures 700 K $< T <$ 900 K. Please note the error bars, which are introduced in Fig. 13 and which are representative for all the ignition delay time measurements of the present work, indicating the uncertainty with respect to measuring the value of ignition delay time ± 10 µs up to ± 100 µs at low temperatures and determining the temperature (± 15 K).

The single components of the GtL surrogate were measured at the same conditions like the GtL and the GtL surrogate to get a better understanding of the differences of the experiments and the simulations. The results are presented together with simulations for these components in Fig. 14. Comparing the simulations and the experiments, the same trends can be observed like the ones for the GtL surrogate. The absolute values of the predicted ignition delay times are too high and the temperature dependence in the NTC region of the simulations is too strong for *n*-decane and *n*-propylcyclohexane. The experimentally determined ignition delay times for *n*-decane and the GtL surrogate are almost identical, see Fig. 14. The

21

differences in the experimental data of *n*-decane, *n*-propylcyclohexane, and the GtL surrogate in the NTC region are smaller than the predicted ones.

Figure 15 shows GtL shock-tube ignition delay measurements of Wang and Oehlschlaeger[11] together with simulations with the mechanism of this work and the mechanisms of Dooley *et al.*[12] and Naik *et al.* [9]. The calculations with the mechanism of the present work show the same trends like the ones with the experimental results of the present work, too long ignition delay times in the whole temperature range and a too strong temperature dependence in the NTC region. The experimental results are also compared to the predictions of other mechanisms. A modified GtL surrogate of Naik *et al.* (28 mol% *iso*-octane, 61 mol% *n*-decane, 11 mol% *n*-dodecane) [9] was used. *N*-dodecane was replaced by the same amount of *n*-decane because *n*-dodecane is only contained in the mechanism of Naik *et al.* [9]. The experimental results in the high temperature region are predicted quite well by the mechanism of Naik *et al.* [9]. At temperatures $T < 1000$ K the predictions of this mechanism differ increasingly compared to the experimental values because it does not include low-temperature chemistry. The simulations with the mechanism of Dooley *et al.* [12] represent the temperature dependence of the experiments very well, the absolute predicted values are about a factor of two higher than the data.

Very similar trends can be observed for the experiments of this work, see Fig. 16. The agreement of the experimental data and the predictions of the mechanism of Naik *et al.* [9] is very well for temperatures $T > 1000$ K. Simulations with the mechanism of Dooley *et al.* [12] predict very well the observed temperature dependence of the experimental ignition delay times with the absolute predicted times being about 50% higher than the measurements.

The examination of the experimental data of *n*-decane allows the comparison to additional mechanisms and explains the performance of the different mechanisms for the GtL surrogates, see Fig. 17. It was shown in Fig. 14 that the experimental ignition delay times of GtL and *n*-

decane are very similar. The ignition of GtL is determined by the *n*-decane chemistry. The addition of branched alkanes, naphthenic or aromatic compounds (*e.g.* 20 mol% of *n*-propylbenzene in the Jet A-1 surrogate) has only a minor influence on the ignition delay times, see Figs. 13-14. Therefore, the ignition delay times of *n*-decane must be reproduced very well by the reaction mechanisms.

The simulation with the mechanism of Naik *et al.* [9] shows a very good agreement with the experiments for temperatures $T > 1000$ K. The mechanism of Honnet *et al.* [13] can predict the measured ignition delay times very well in the whole temperature range, only for $T < 740$ K too long ignition delay times are predicted. The simulations with the mechanism of Dooley *et al.* [12] represent the measured ignition delay time quite well especially in the NTC region where almost a perfect agreement of experiments and simulations can be observed. The predictions with the mechanism of Sarathy *et al.* [43] predict too long ignition delay at high temperatures and slightly too short values in the NTC region. For temperatures $T < 830$ K the temperature dependence of the experimental values is well represented by this mechanism. We could only use the mechanisms of Naik *et al.* [9] and Dooley *et al.* [12] for the comparison with the GtL data because they are the only mechanisms which include *n*-decane and *iso*-octane chemistry. The good prediction capability of these mechanisms is caused by their good representation of the *n*-decane ignition chemistry.

Measurements and calculations have shown that the addition of *iso*-alkanes, naphthenes, and aromatics, in reasonable amounts, has only a minor influence on ignition delay time. Thus, the addition of further compounds considered to be important to represent characteristic properties such as aromatic content, sooting propensity, smoke point, derived cetane number, and boiling behavior to the surrogates, do not significantly influence ignition. Obviously, the combustion characteristics are well-predicted as long as the *n*-alkanes sub-mechanism is correct.

Table 3. Averaged pressure profile used as basis for the simulations of all shock tube experiments.

| Reaction time $t / \mu s$ | pressure profile $p / p_0$ |
|---|---|
| 0 | 1.000 |
| 50 | 1.004 |
| 250 | 1.027 |
| 450 | 1.046 |
| 650 | 1.062 |
| 850 | 1.072 |
| 1050 | 1.088 |
| 1250 | 1.101 |
| 1450 | 1.127 |
| 1650 | 1.157 |
| 1850 | 1.170 |
| 2050 | 1.160 |
| 2250 | 1.152 |
| 2450 | 1.153 |
| 2650 | 1.148 |
| 2850 | 1.143 |
| 3050 | 1.139 |
| 3250 | 1.136 |
| 3450 | 1.140 |
| 3650 | 1.142 |
| 3850 | 1.142 |
| 4050 | 1.153 |
| 4250 | 1.161 |
| 4450 | 1.168 |
| 4650 | 1.165 |
| 4850 | 1.166 |
| 5050 | 1.168 |
| 5250 | 1.170 |

| | |
|---|---|
| 5450 | 1.172 |
| 5650 | 1.175 |
| 5850 | 1.175 |
| 6050 | 1.178 |
| 6250 | 1.181 |
| 6450 | 1.184 |
| 6650 | 1.187 |
| 6850 | 1.189 |
| 7050 | 1.189 |
| 7250 | 1.188 |
| 7450 | 1.188 |
| 7650 | 1.190 |
| 7850 | 1.192 |
| 8000 | 1.192 |
| 10000 | 1.192 |

**4.3 Burning velocities**

Experimentally determined laminar burning velocities of GtL, its surrogate, and of Jet A-1 burning in air, at ambient pressure and a preheat temperature of 473 K, are plotted in Fig. 18. The burning velocities of the GtL itself agree, within the uncertainty range, with those of the GtL surrogate prepared from the same surrogate composition that has been used in modeling, although they are about 5% smaller. The small variation in the burning velocities of the pure GtL mixture and the GtL surrogate mixture reflects the suitability of the selected surrogate model. Our measurements were restricted to the fuel stoichiometry $\varphi = 1.0 - 1.5$ due to the reasons discussed earlier. The burning velocities increase with fuel stoichiometry and peak at slightly rich condition, namely $\varphi = 1.05$. Recently, Vukadinovic *et al.* reported on laminar burning velocities of a GtL and GtL blends measured in spherical expanding flames, for a variety of initial temperature conditions. The measurements of the present work are in close agreement with those of Vukadinovic *et al.* [18], at stoichiometric and at fuel rich

conditions, as to be seen from Fig. 18. At very rich conditions, their measurements were slightly larger than ours, although still within the uncertainty limits. The comparison between experimentally derived and predicted laminar flame speeds of the GtL mixtures is also included in Fig. 18. The kinetic model (line) closely predicts the measured flame speeds of the pure GtL (full triangles) and of the GtL surrogate (full squares), within the experimental uncertainty range and the entire fuel air range studied ($0.7 < \phi < 1.5$). Measurements of Jet A-1, included in Fig. 18 as well, also feature similar flame velocities compared with those of the GtL mixtures. It should be stated that the measured burning velocities of GtL of the present work agree, within the uncertainty range, with the one of CtL (Coal to Liquid) measured earlier [21]

Sensitivity analyses concerning laminar flame speeds of the GtL-mixtures (neat and surrogate) were performed yielding results similar to those obtained earlier for the combustion of a CtL fuel [21]. As anticipated and typical for hydrocarbon flames, the two most sensitive reactions are the chain branching reaction between H atoms and molecular oxygen ($H + O_2 \rightleftarrows OH + O$) and the reaction governing heat release ($CO + OH \rightleftarrows CO_2 + H$). Furthermore, reactions of the H/O- and CO-sub-systems and those of $C_2H_x$ and $C_3H_x$ species stemming mostly from the combustion of large alkanes were found to be of minor importance with respect to laminar flame speeds, similar to reactions involving higher hydrocarbons.


## 5. CONCLUSIONS

The oxidation kinetics of a Gas-to-Liquid Fully Synthetic Jet Fuel (GtL-FT-SPK) and of a GtL surrogate mixture were studied using complementary laboratory experimental rigs operating over a wide range of conditions: a JSR (at $p = 10$ bar and a constant residence time of 1 s, $770 < T/K < 1070$, and for variable equivalence ratios $0.5 < \varphi < 2$), a shock tube (at $p$ around 16 bar, $650 < T/K < 1400$, $\varphi = 0.5$ and $\varphi = 1$), and a conical flame burner (at $p = 1$ bar

and a preheat temperature of 473 K, $\varphi = 1.0 - 1.5$). In the JSR, mole fractions of reactants, stable intermediates, and final products were measured versus temperature by probe sampling followed by on-line and off-line gas chromatography analyses and on-line Fourier Transformed Infra-Red spectrometry. Ignition delay times were measured behind reflected shock waves by recording time-dependent CH* emission at 431 nm. Burning velocities were obtained by applying the cone angle method. These results were compared to corresponding data obtained for the oxidation, ignition and combustion of the two GtL-mixtures (neat and surrogate) and Jet A-1. Although differences appeared, mainly in terms of intermediate products concentrations, the data showed strong similarity concerning the combustion characteristics considered of the pure GtL, the GtL surrogate and the Jet A-1.

The GtL- oxidation under these conditions was modeled using a detailed kinetic reaction mechanism and a simple surrogate model fuel *(n*-decane, *iso*-octane, and *n*-propylcyclohexane)*. The validity of the kinetic scheme was also shown by comparing new data obtained in a JSR for the oxidation of a fuel having the exact composition of the model fuel. Burning velocities were also simulated. A good representation of the GtL oxidation kinetics was obtained. Future modeling improvements could be achieved by using a more complex model fuel which should include more realistic alkanes and naphthenes. The kinetics for such model fuel blends have recently been proposed [39, 43-45].

Concerning the comparison between measured and predicted ignition delay time of GtL, too long ignition delay times are predicted by the model of the present work, in particular for the NTC regime. Obviously, the decane sub-model is too slow and needs improvements. The predicted laminar burning velocities agree very well with the experimental results.

For the conditions investigated in this study, the GtL ignition delay times and burning velocities agree with those for the GtL surrogate and with corresponding data for petrol-derived jet fuel. This information is significant due to its impact on combustor design.

Ignition delay knowledge is also important to estimate risks of flashback or auto-ignition incidence. The present findings support the potential for the GtL mixture investigated to serve as an alternative aviation fuel. Finally, the present results will contribute to optimizing synthetic jet fuel mixtures for aero jet combustors.

**Supplementary Information**

The proposed chemical kinetic reaction mechanism in CHEMKIN format, the associated thermochemical and transport data in CHEMKIN format.
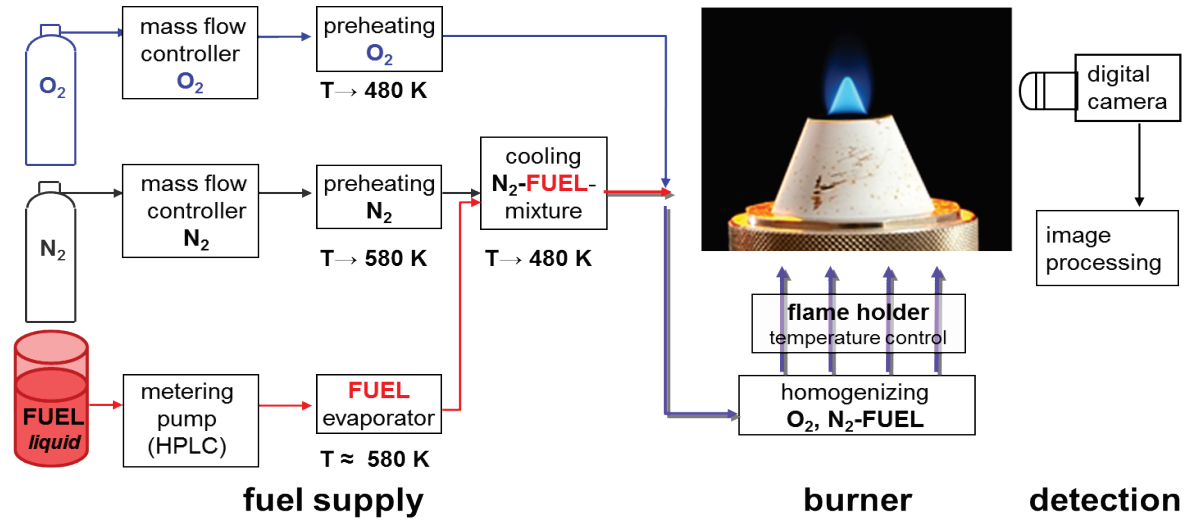
**Figures**



Figure 1. Experimental set up used for determining burning velocity of a liquid fuel.
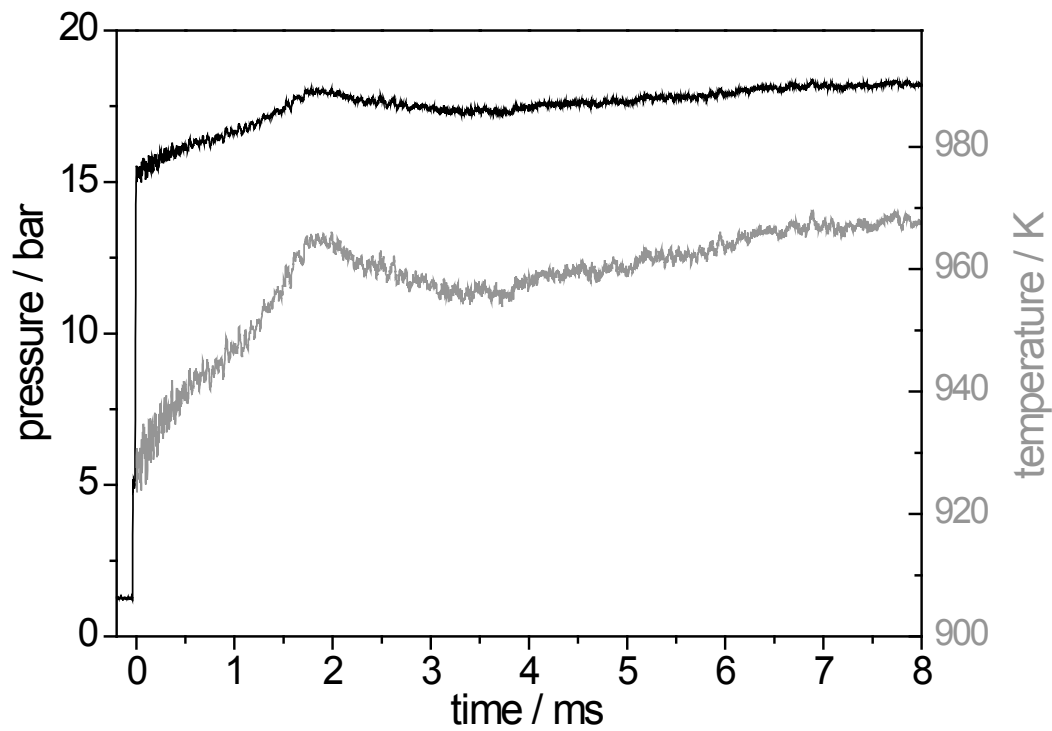
Figure 2. Typical pressure (black line) and derived temperature (grey line) profile assuming adiabatic isentropic compression obtained for a non-igniting fuel / air mixture (dilution 1:2) at the following conditions: $T_{5,\text{initial}} = 929$ K and $p_{5,\text{initial}} = 15.30$ bar.
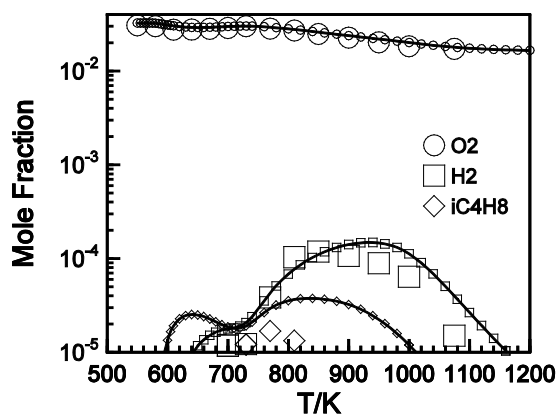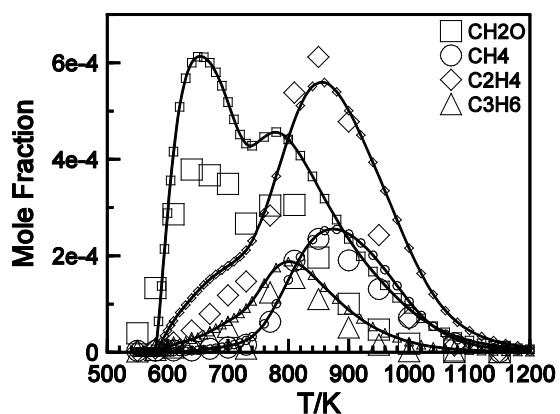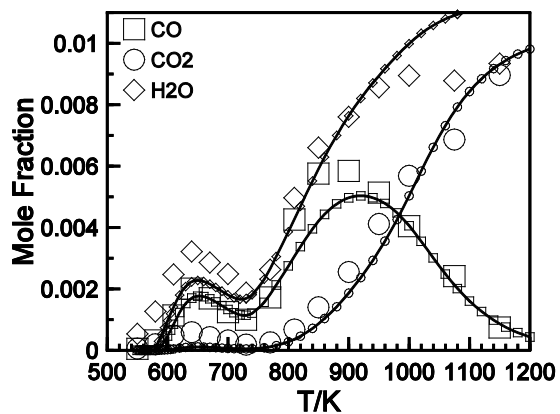
Figure 3. GtL- oxidation in a JSR at $\varphi = 0.5$, $p = 10$ bar, and $t = 1$ s (Data: large symbols, model fuel #1 simulations: lines and small symbols).
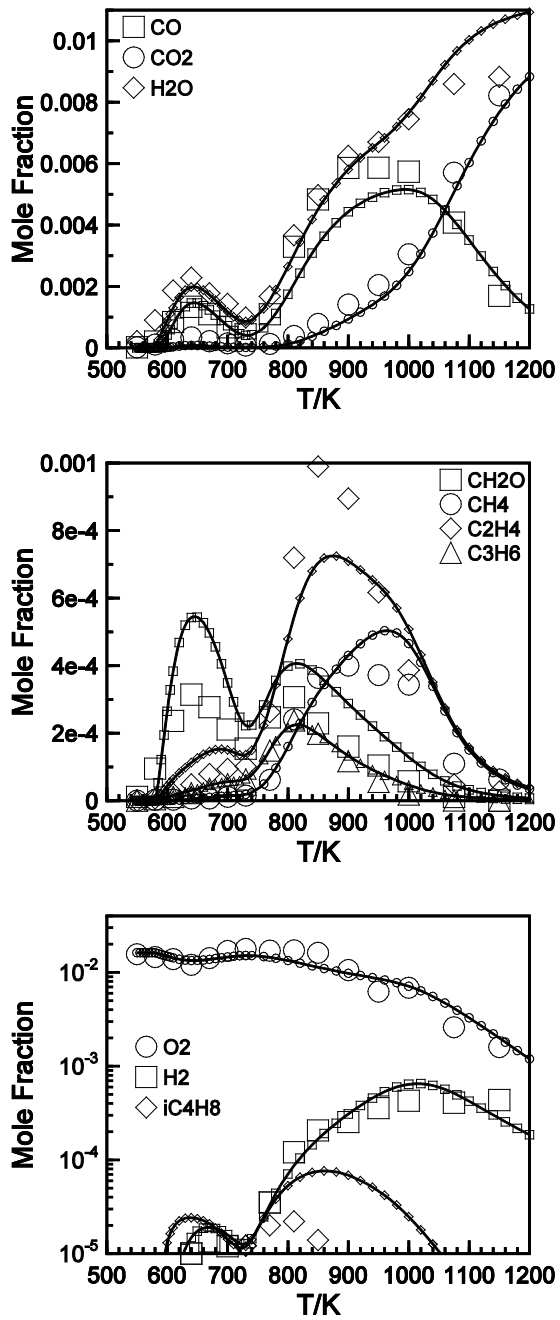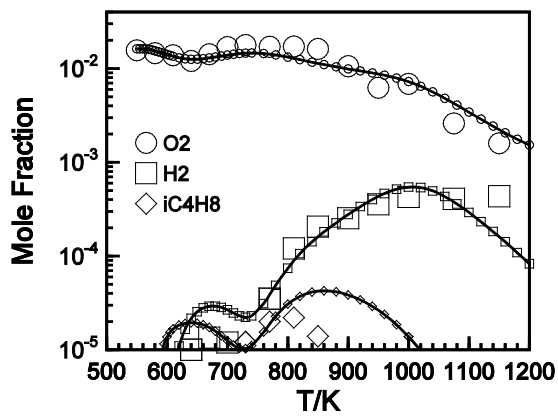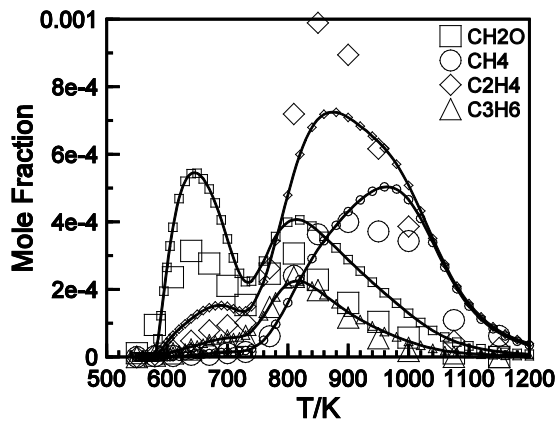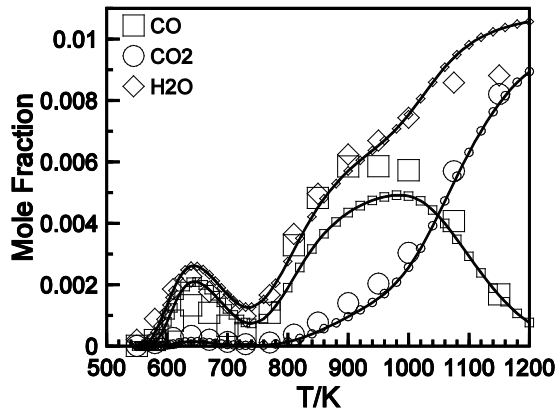
Figure 4. GtL-oxidation in a JSR at $\varphi = 1.0$, $p = 10$ bar, and $t = 1$ s (Data: large symbols, model fuel #1 simulations: lines and small symbols).
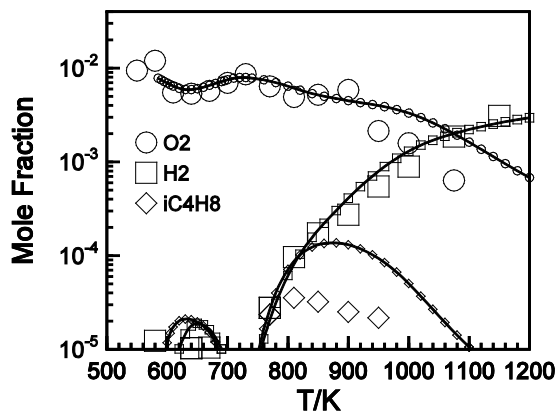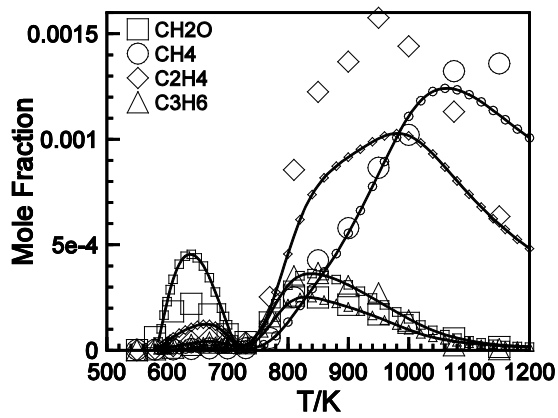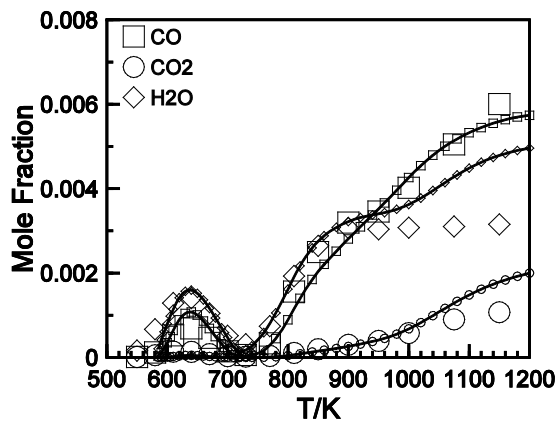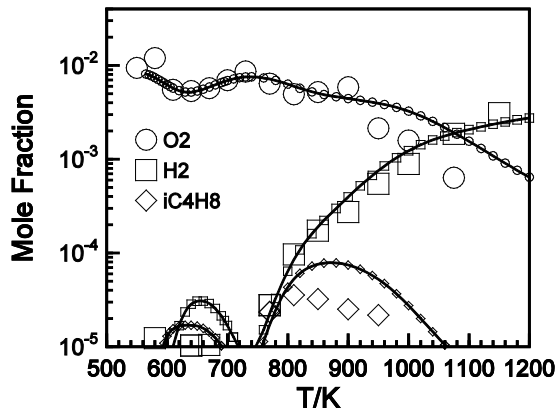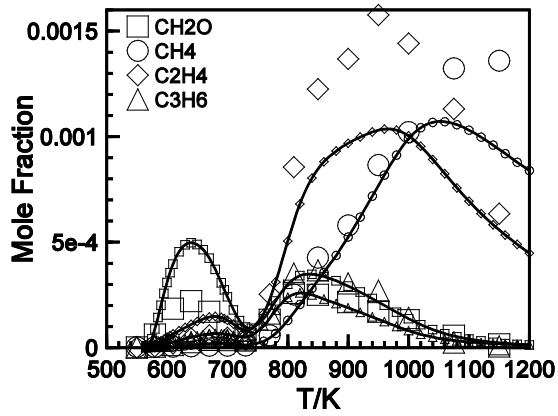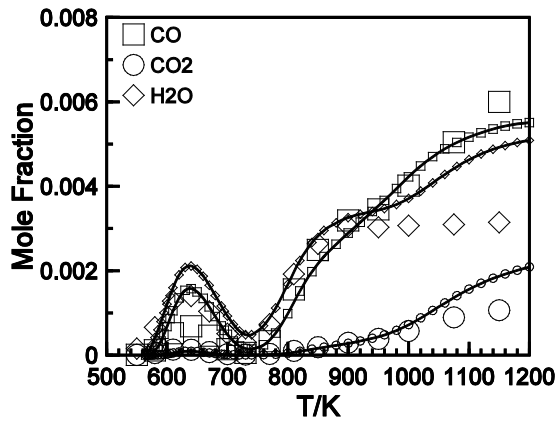
Figure 5. GtL- oxidation in a JSR at $\varphi = 2.0$, $p = 10$ bar, and $t = 1$ s (Data: large symbols, model fuel #1 simulations: lines and small symbols).
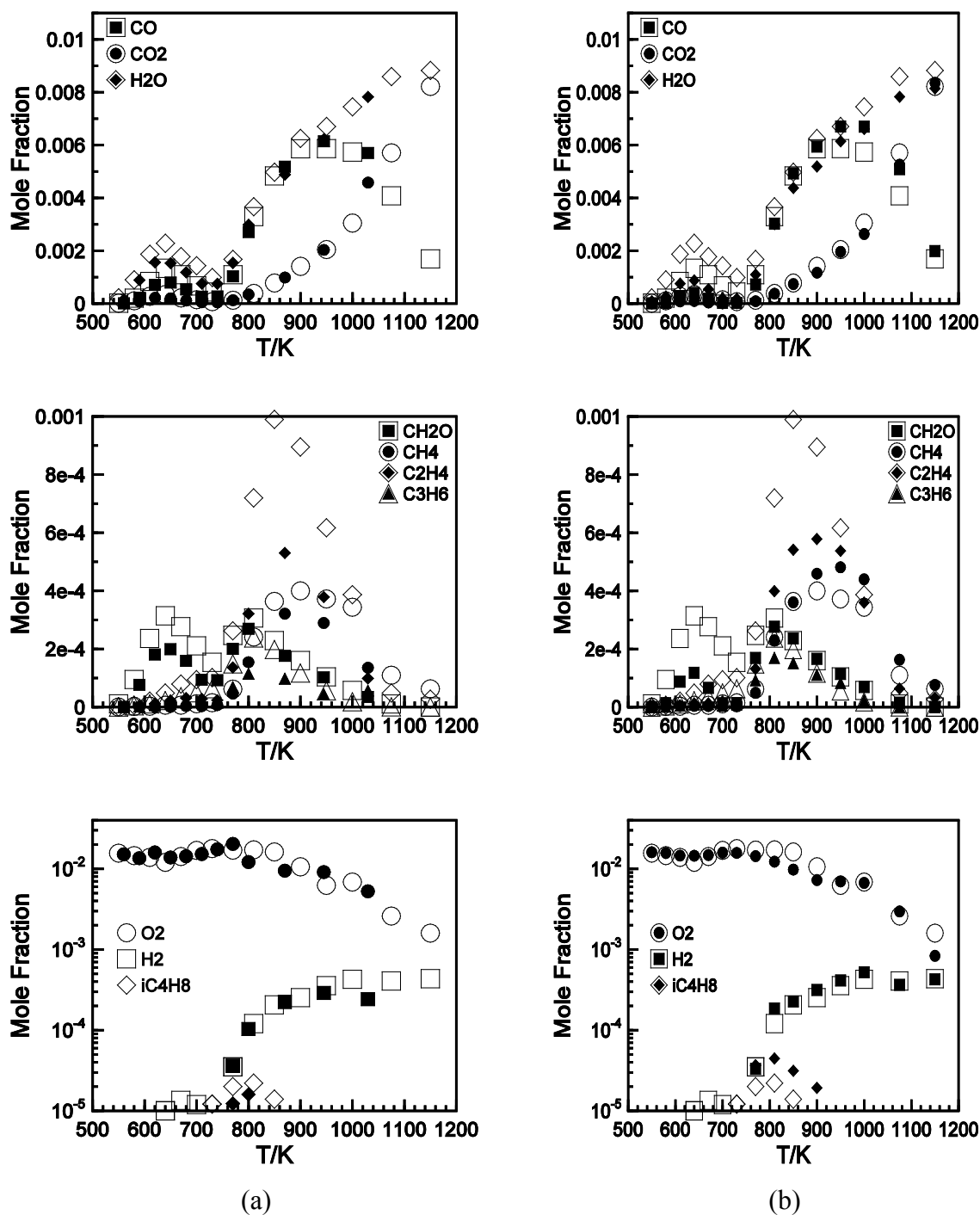
Figure 6. Comparison of experimental data obtained in a JSR for the oxidation of (a) Jet A-1 (closed symbols) and GtL (open symbols) and (b) CtL (closed symbols) [21] and GtL jet fuel (open symbols) at $\varphi = 1.0$, $p = 10$ bar, and $t = 1$ s. The initial fuel concentration was 1000 ppm. The CtL provided by Sasol ($C_{11.06}H_{21.6}$, M = 154.32 g mol$^{-1}$, density = 815.7 g l$^{-1}$) has a mass composition of 36.3% *iso*-alkanes, 5.7% *n*-alkanes, 16.1% mono-naphthenes, 28.3% di-/tri-naphthenes, 4% mono-aromatics, and 9.6% naphthenoaromatics) whereas the GtL provided by Shell ($C_{10.45}H_{23.06}$, M = 148.44 g·mol$^{-1}$, density = 737.7 g l$^{-1}$) has a mass composition of 62.8% *iso*-alkanes, 28.1% *n*-alkanes, 0.6% mono-naphthenes, 8.2% di-naphthenes, and 0.2% mono-aromatics)
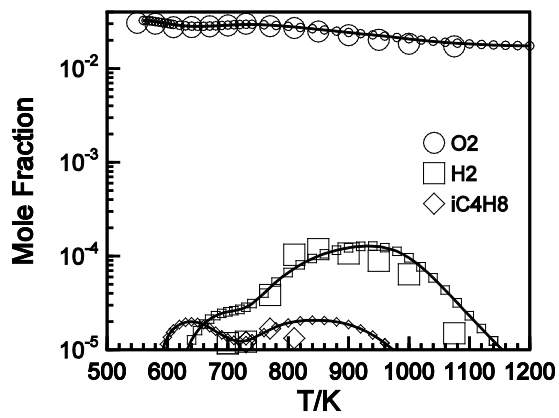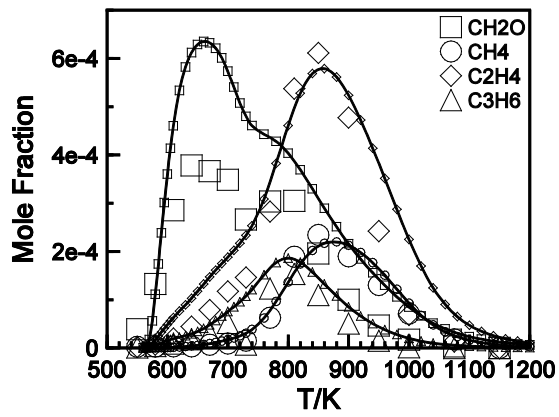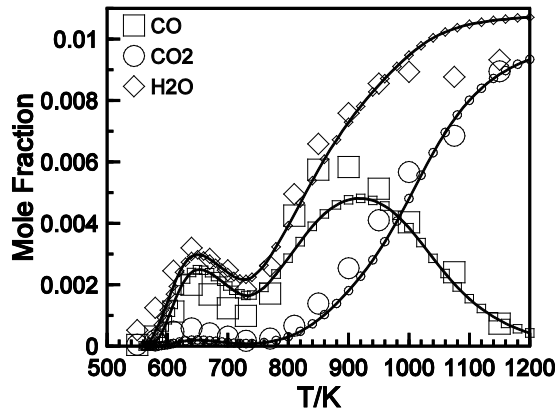
Figure 7. GtL- oxidation in a JSR at $\varphi = 0.5$, $p = 10$ bar, and $t = 1$ s (Data: large symbols, model fuel #2 simulations: lines and small symbols).

Figure 8. GtL-oxidation in a JSR at $\varphi = 1.0$, $p = 10$ bar, and $t = 1$ s (Data: large symbols, model fuel #2 simulations: lines and small symbols).
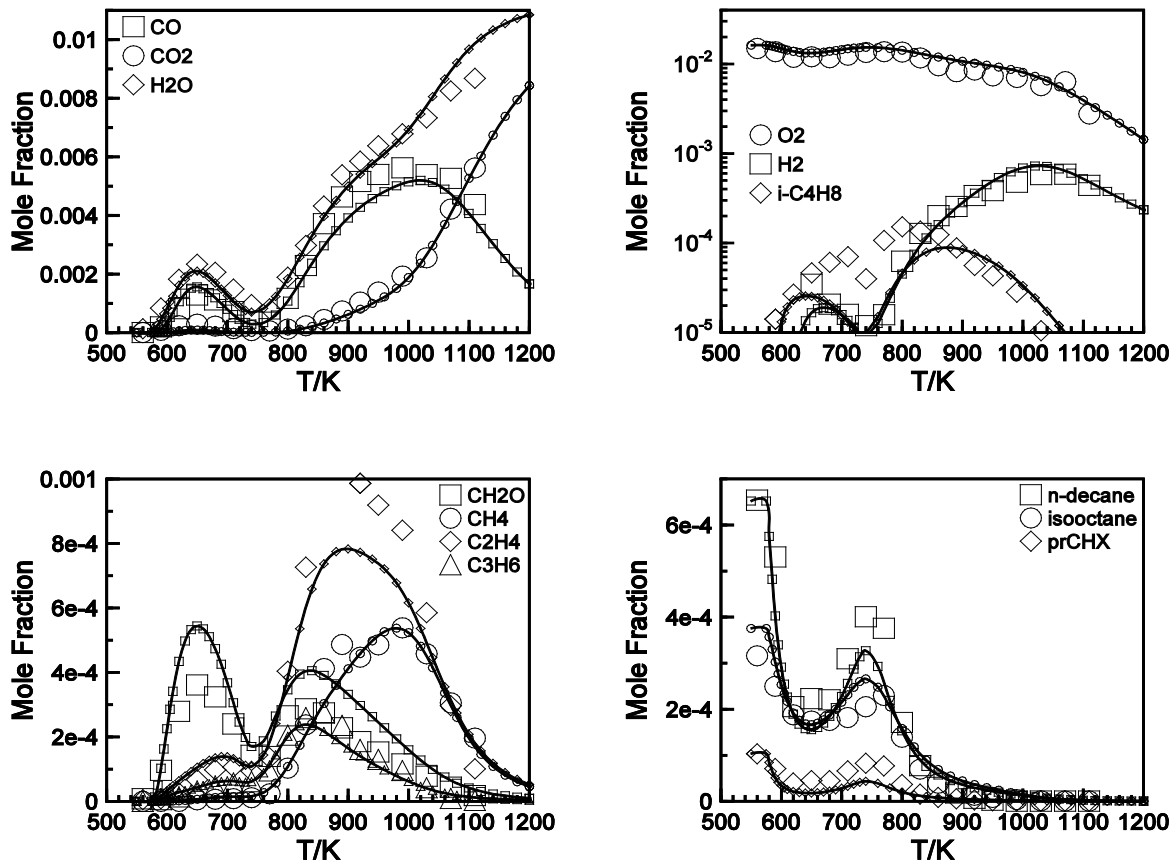
Figure 9. GtL- oxidation in a JSR at $\varphi = 2.0$, $p = 10$ bar, and $t = 1$ s (Data: large symbols, model fuel #2 simulations: lines and small symbols).

Figure 10. The oxidation of the model fuel #1 in a JSR at $\varphi = 1.0$, $p = 10$ bar, and $t = 0.7$ s (Data: large symbols, simulations: lines and small symbols). The same fuel composition was used both in the experiments and in the modeling.
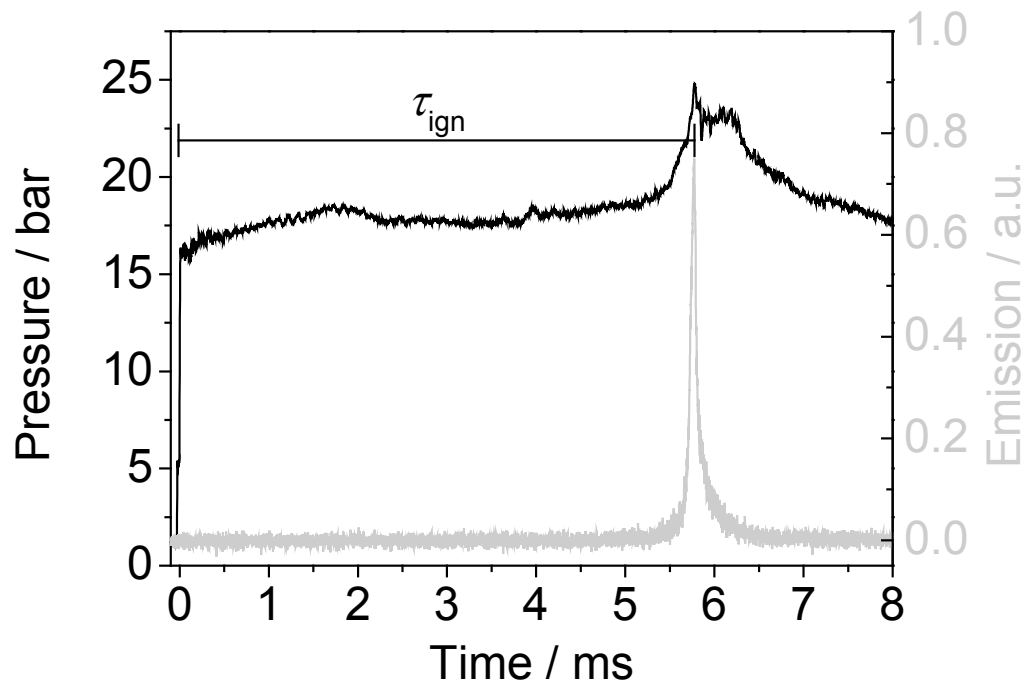
Figure 11. Typical pressure (black line) and CH* emission (grey line) profiles of a GtL / $O_2$ / $N_2$ mixture ($\varphi = 0.5$, dilution 1:2) at $T_5 = 920$ K and $p_5 = 16.1$ bar.
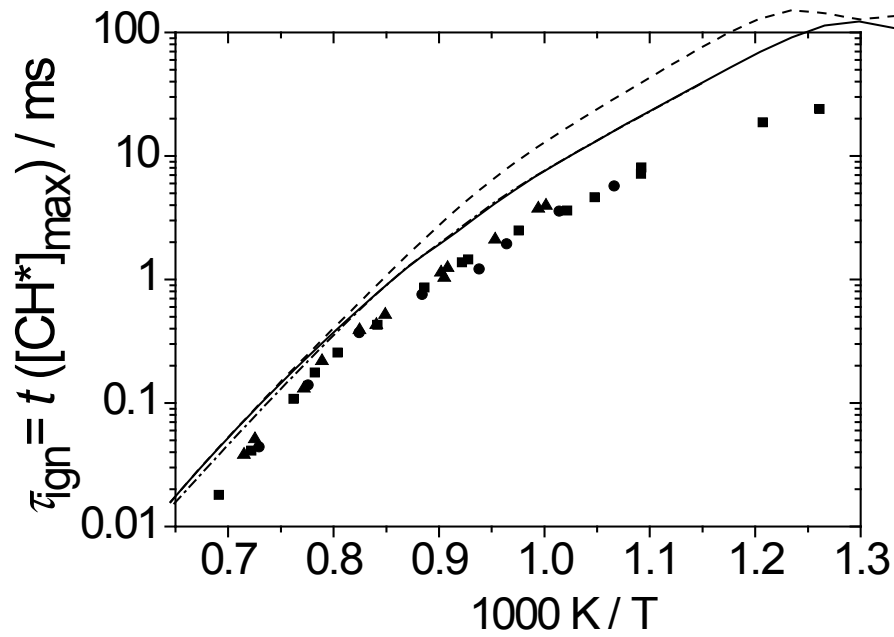
Figure 12. Ignition delay time: Comparison between measurements (symbols ; GtL: circles; GtL-surrogate: squares; Jet A-1: triangles) and predictions (lines) for various fuel-air mixtures diluted in $N_2$ (1:2) at $\varphi = 0.5$ and $p = 16$ bar: solid line: GtL-surrogate with pressure profile, dashed line: GtL-surrogate with constant pressure/ temperature, dashed-dotted line: Jet A-1 surrogate with pressure profile.
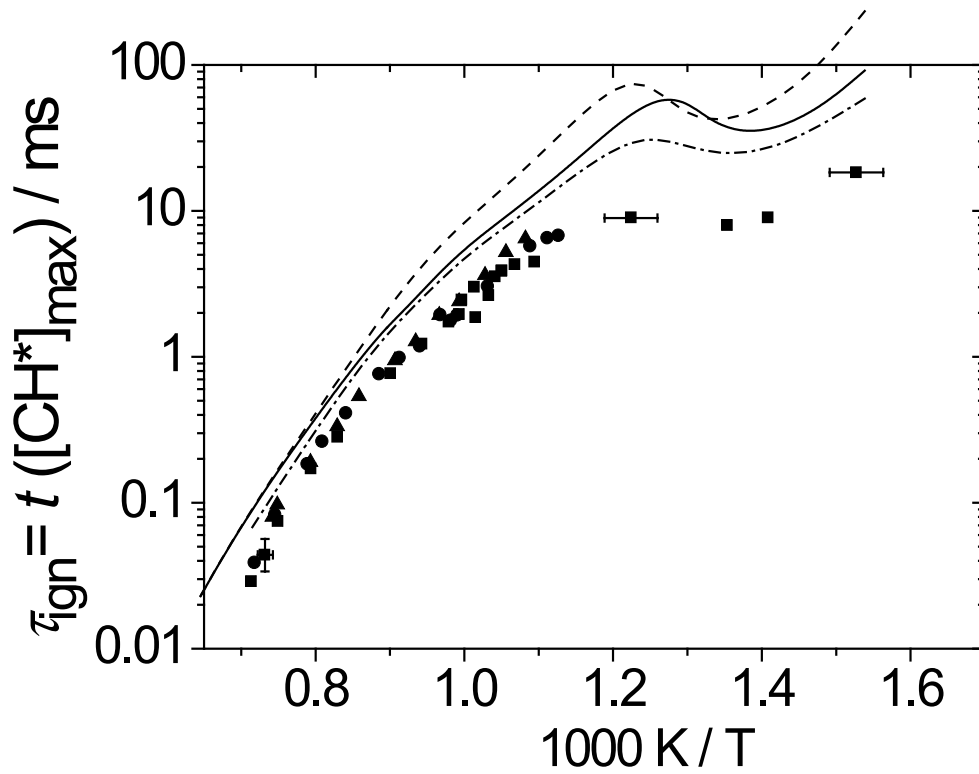
Figure 13. Ignition delay time: Comparison between measurements (symbols; GtL: circles; GtL-surrogate: squares; Jet A-1: triangles) and predictions (lines) for various fuel-air mixtures diluted in $N_2$ (1:2) at $\varphi = 1.0$ and $p = 16$ bar: solid line: GtL-surrogate with pressure profile, dashed line: GtL-surrogate with constant pressure/ temperature, dashed-dotted line: Jet A-1 surrogate with pressure profile.
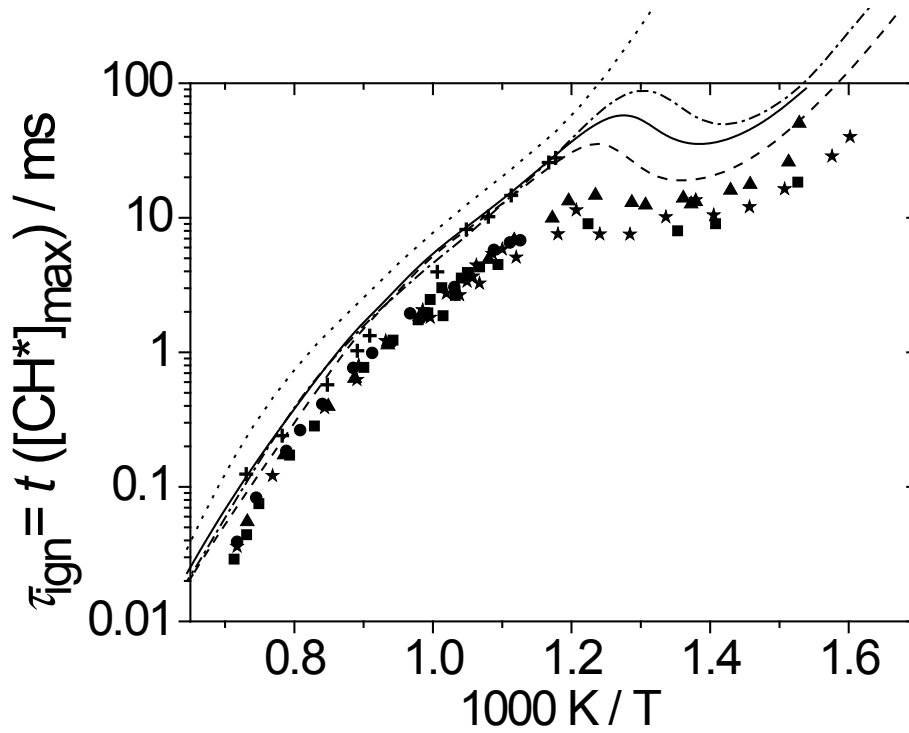
Figure 14. Ignition delay time: Comparison between measurements (symbols; GtL: circles; GtL-surrogate: squares; *n*-propylcyclohexane: triangles; *n*-decane: stars, *iso*-octane: crosses) and predictions (lines) for various fuel-air mixtures diluted in $N_2$ (1:2) at $\varphi = 1.0$ and $p = 16$ bar: solid line: GtL-surrogate with pressure profile, dashed line: *n*-decane with pressure profile, dashed-dotted line: *n*-propylcyclohexane with pressure profile, dotted line: *iso*-octane with pressure profile.
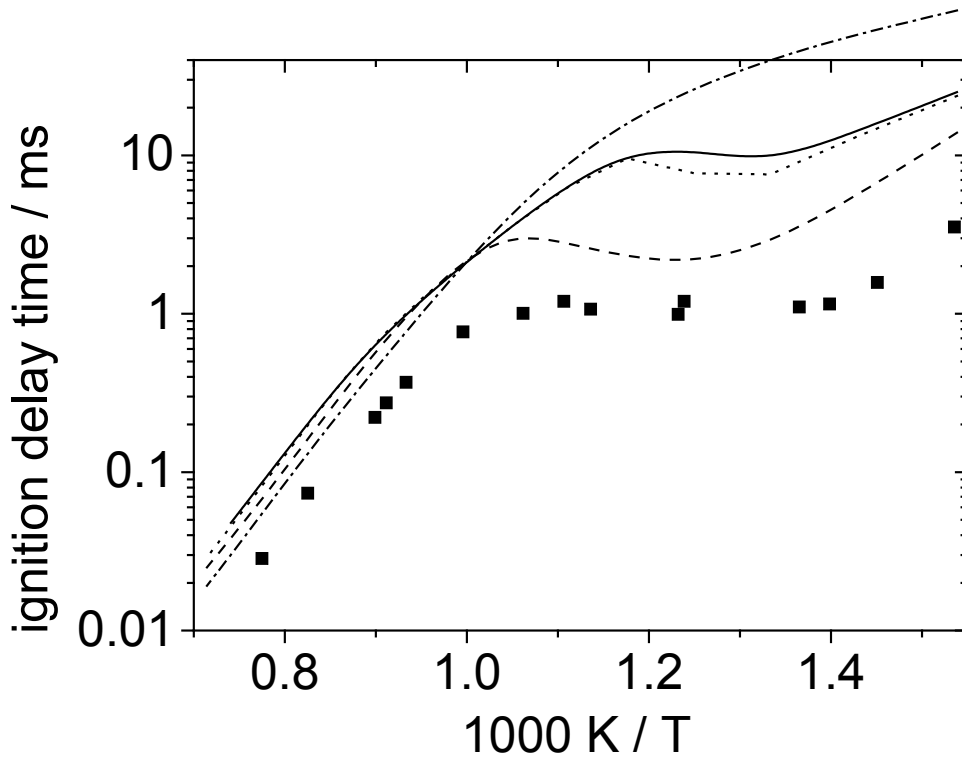
Figure 15. Ignition delay time: Comparison between measurements of GtL (symbols, Wang and Oehlschlaeger [11]) at $\varphi = 1.0$, $p = 16$ bar and undiluted conditions and predictions with different mechanisms and surrogates (lines) considering the pressure increase of $(\mathrm{d}p/\mathrm{d}t)\cdot(1/p_0) = 3\%$ / ms. Solid line: reaction mechanism and composition of GtL-surrogate of present work; dotted line: reaction mechanism of present work and modified GtL-surrogate of Naik *et al.* [9] (28 mol% *iso*-octane, 72 mol% *n*-decane); dashed line: reaction mechanism of Dooley *et al.* [12]; and modified GtL-surrogate of Naik *et al.* [9], dashed-dotted line: reaction mechanism and modified GtL-surrogate of Naik *et al.* [9].
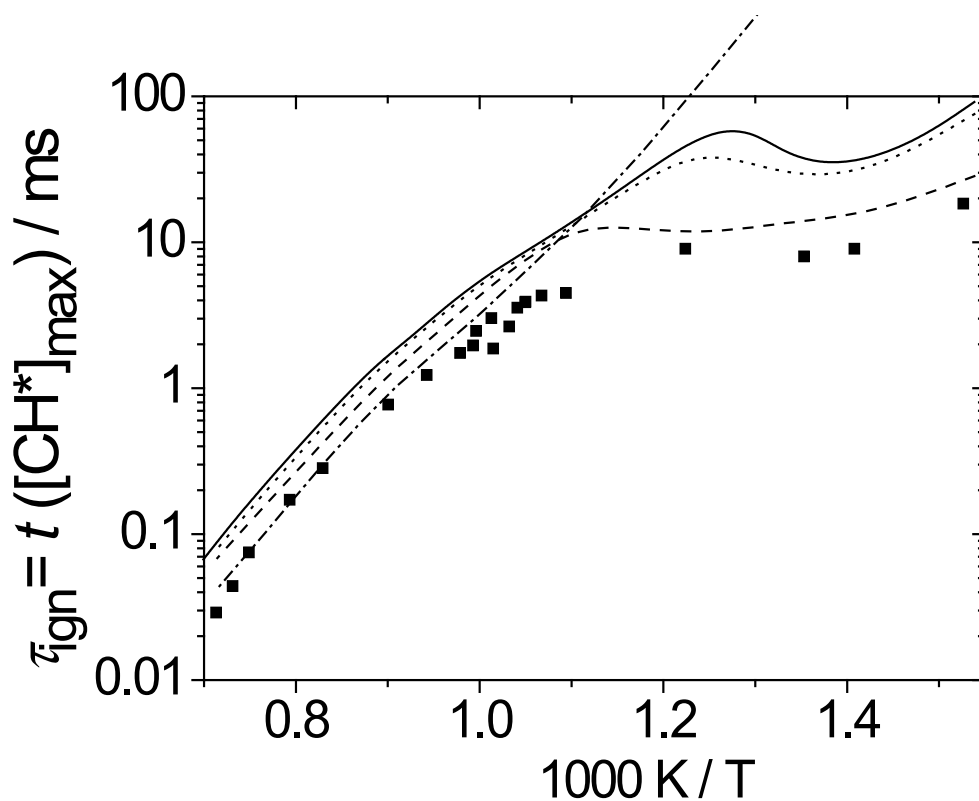
Figure 16. Ignition delay time: Comparison between the measurements (present work) of GtL-surrogate (squares) and predictions (lines) with different mechanisms and GtL-surrogates (lines), at $\varphi = 1.0$, $p = 16$ bar diluted by $N_2$ (1:2). Solid line: reaction mechanism and composition of GtL-surrogate of present work; dotted line: reaction mechanism of present work; modified composition of GtL-surrogate of Naik *et al.* [9] (28 mol% *iso*-octane, 72 mol% *n*-decane); dashed line: reaction mechanism of Dooley *et al.* [12] and modified composition of GtL-surrogate of Naik *et al.* [9]; dashed-dotted line: reaction mechanism and modified GtL-surrogate of Naik *et al.* [9].
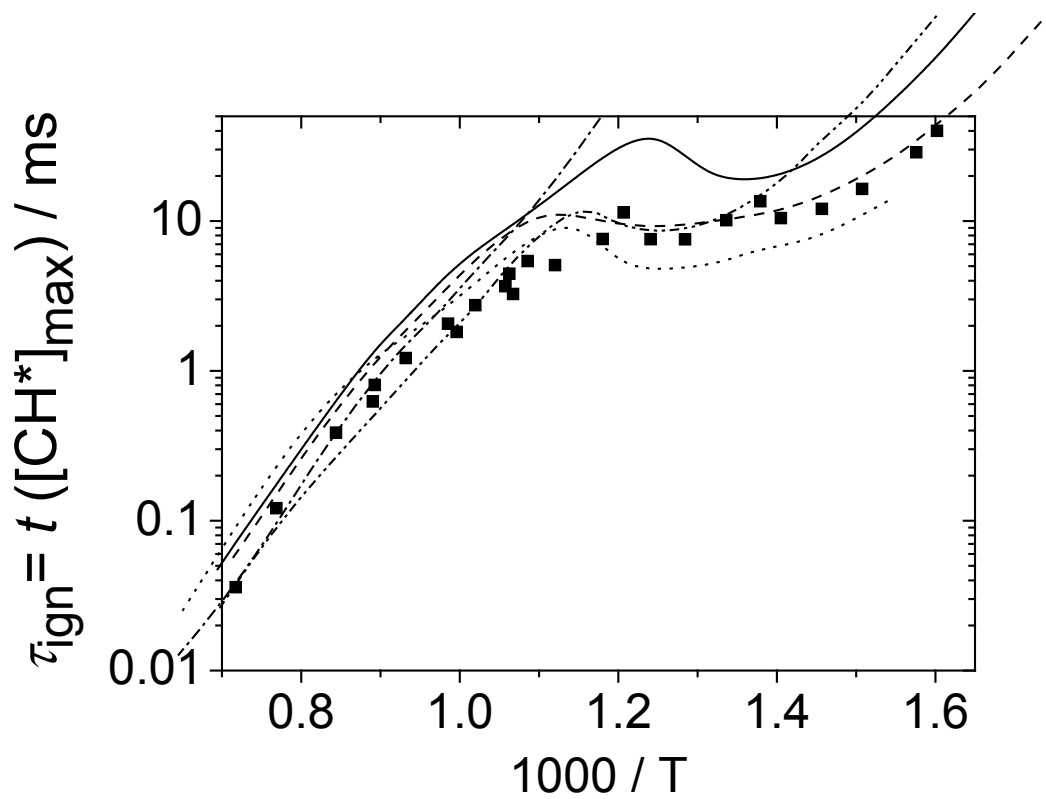
Figure 17. Ignition delay time: Comparison between measurements (symbols: *n*-decane) and predictions (lines) using several reaction mechanisms at $\varphi = 1.0$, $p = 16$ bar diluted in $N_2$ (1:2). Solid line: mechanism of present work; dashed line: mechanism of Dooley *et al.* [12], dotted line: mechanism of Sarathy *et al.* [43], dashed-dotted line: mechanism of Naik *et al.* [9], dashed-double dotted line: mechanism of Honnet *et al.* [13].
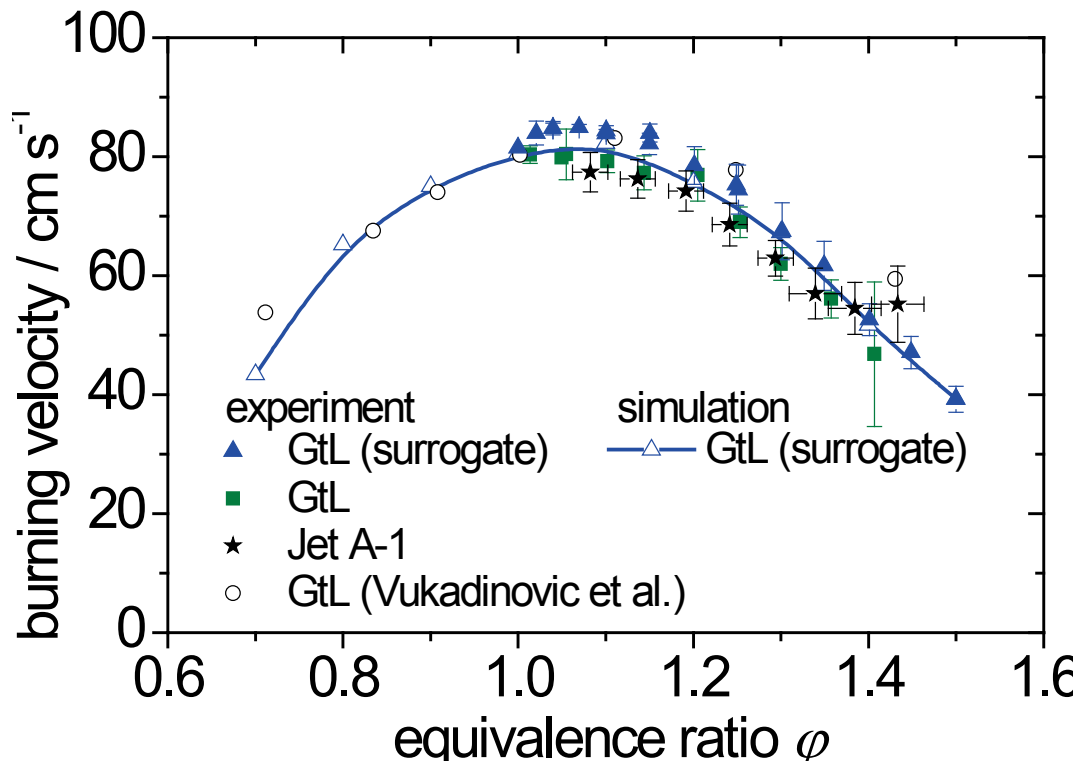
Figure 18. Comparison of measured burning velocities (symbols) and predicted laminar flame speeds (line, open triangles) of various fuel-air-mixtures at $T_0 = 473$ K and $p = 1$: GtL-full squares; GtL-surrogate – full triangles; Jet A-1 – stars; GtL-  – circles, Vukadinovic *et al.* [18].

# REFERENCES

1.	EIA, in: *The International Energy Outlook*, U.S. Energy Information Administration (EIA): Washington, D.C, 2011.
2.	IEA World Energy Outlook 2011. OECD/IEA, Paris. www.worldenergyoutlook.org
3.	European-Commission. Biofuels flight path. http://ec.europa.eu/energy/renewables/biofuels/doc/20110622_biofuels_flight_path_technical_paper.pdf.
4.	P. Dagaut; M. Cathonnet, Prog. Energy Combust. Sci. 32 (1) (2006) 48-92.
5.	ASTM, in: *Standard Specification for Aviation Turbine Fuels*, 2011; Vol. D1655.
6.	C. Wahl; M. Kapernaum, in: 2000.
7.	U. Steil; M. Braun-Unkhoff; M. Aigner in: 46th AIAA Aerospace Science Meeting AIAA-2008-0973, Reno, Nevada, USA, 7 - 10 Jan, 2008; Reno, Nevada, USA, 2008.
8.	S. Dooley; S. H. Won; M. Chaos; J. Heyne; Y. G. Ju; F. L. Dryer; K. Kumar; C. J. Sung; H. W. Wang; M. A. Oehlschlaeger; R. J. Santoro; T. A. Litzinger, Combust. Flame 157 (12) (2010) 2333-2339.
9.	C. V. Naik; K. V. Puduppakkam; A. Modak; E. Meeks; Y. L. Wang; Q. Y. Feng; T. T. Tsotsis, Combust. Flame 158 (3) (2011) 434-445.
10.	X. Hui; K. Kumar; C. J. Sung; T. Edwards; D. Gardner, Fuel 98  (2012) 176-182.
11.	H. W. Wang; M. A. Oehlschlaeger, Fuel 98  (2012) 249-258.
12.	S. Dooley; S. H. Won; S. Jahangirian; Y. G. Ju; F. L. Dryer; H. W. Wang; M. A. Oehlschlaeger, Combust. Flame 159 (10) (2012) 3014-3020.
13.	S. Honnet; K. Seshadri; U. Niemann; N. Peters, Proc. Combust. Inst. 32 (1) (2009) 485-492.
14.	T. Edwards; L. Q. Maurice, J. Propul. Power 17 (2) (2001) 461-466.
15.	B. M. Gauthier; D. F. Davidson; R. K. Hanson, Combust. Flame 139 (4) (2004) 300-311.
16.	S. S. Vasu; D. E. Davidson; R. K. Hanson, Combust. Flame 152 (1-2) (2008) 125-143.
17.	T. Kick; J. Herbst; T. Kathrotia; J. Marquetand; M. Braun-Unkhoff; C. Naumann; U. Riedel, Energy 43 (1) (2012) 111-123.
18.	V. Vukadinovic; P. Habisreuther; N. Zarzalis in: *Experimental study on combustion characteristics of conventional and alternative liquid fuels*, ASME Turbo Expo, Copenhagen, Denmark June 11-15, 2012; ASME: Copenhagen, Denmark 2012; pp GT2012-69449.
19.	V. Vukadinovic; P. Habisreuther; N. Zarzalis, J. Eng. Gas Turbines Power-Transact. of the Asme 134 (12) (2012)
20.	C. S. Ji; Y. L. Wang; F. N. Egolfopoulos, J. Propul. Power 27 (4) (2011) 856-863.
21.	A. Mzé Ahmed; P. Dagaut; K. Hadj-Ali; G. Dayma; T. Kick; J. Herbst; T. Kathrotia; M. Braun-Unkhoff; J. Herzler; C. Naumann; U. Riedel, Energy Fuels 26 (10) (2012) 6070−6079.
22.	P. Dagaut; M. Cathonnet; J. P. Rouan; R. Foulatier; A. Quilgars; J. C. Boettner; F. Gaillard; H. James, Journal of Physics E-Scientific Instruments 19 (3) (1986) 207-209.
23.	P. Dagaut, J. Eng. Gas Turbines Power-Transact. of the Asme 129 (2) (2007) 394-403.
24.	P. Dagaut; A. El Bakali; A. Ristori, Fuel 85 (7-8) (2006) 944-956.
25.	J. Herzler; L. Jerig; P. Roth, Proc. Combust. Inst. 30 (1) (2005) 1147-1153.
26.	G. E. Andrews; D. Bradley, Combust. Flame 18 (1) (1972) 133-153.
27.	A. Freund; G. Friedrich; C. Merten; G. Eigenberger, Chem. Ing. Tech. 78 (5) (2006) 577-580.
28.	T. Edwards; J. V. Atria in: *Thermal Stability of High Temperature Fuels*, ASME Turbo Expo, Orlando, Florida, USA, June 2-5, 1997; ASME: Orlando, Florida, USA, 1997; pp GT1997-143.
29.	C. K. Law, Symposium (International) on Combustion 22 (1) (1989) 1381-1402.
30.	C. J. Rallis; A. M. Garforth, Prog. Energy Combust. Sci. 6 (4) (1980) 303-329.
31.	C. K. Wu; C. K. Law, Symposium (International) on Combustion 20 (1) (1985) 1941-1949.
32.	G. H. Markstein, Non-Steady Flame Propagation, Pergamon, New York (USA), 1964, p.^pp. 22.
33.	R. J. Kee; F. M. Rupley; J. A. Miller, in: *SAND87-8215*, Sandia National Laboratories: Livermore, CA, 1987.
34.	R. J. Kee; F. M. Rupley; J. A. Miller, in: *SAND89-8009*, Sandia National Laboratories: Livermore, CA, 1989.
35.	P. Glarborg; R. J. Kee; J. F. Grcar; J. A. Miller, in: *SAND86-8209*, Sandia National Laboratories: Livermore, CA, 1986.
36.	A. Mze-Ahmed; K. Hadj-Ali; P. Dievart; P. Dagaut, Energy Fuels 24  (2010) 4904-4911.
37.	J. Herzler; C. Naumann, Proc. Combust. Inst. 32 (1) (2009) 213-220.
38.	R. J. Kee; G. J.F.; S. M.D.; J. A. Miller, in: *SAND85-8240*, Sandia National Laboratories: Livermore, CA, 1985.
39.	A. Mze-Ahmed; K. Hadj-Ali; P. Dagaut; G. Dayma, Energy Fuels 26 (7) (2012) 4253-4268.
40.	SWAFEA, in: Sustainable way for alternative fuels and energy for aviation, EU, 2012.

41.     A. E. Lutz; R. J. Kee; J. A. Miller, in: *SAND87-8248*, Sandia National Laboratories: Livermore, CA, 1987.

42.     P. Dagaut; S. Gail, J. Phys. Chem. A 111 (19) (2007) 3992-4000.

43.     S. M. Sarathy; C. K. Westbrook; M. Mehl; W. J. Pitz; C. Togbe; P. Dagaut; H. Wang; M. A. Oehlschlaeger; U. Niemann; K. Seshadri; P. S. Veloo; C. Ji; F. N. Egolfopoulos; T. Lu, Combust. Flame 158 (12) (2011) 2338-2357.

44.     F. Karsenty; S. M. Sarathy; C. Togbé; C. K. Westbrook; G. Dayma; P. Dagaut; M. Mehl; W. J. Pitz, Energy Fuels 26 (8) (2012) 4680-4689.

45.     P. Dagaut; A. Ristori; A. Frassoldati; T. Faravelli; G. Dayma; E. Ranzi, Proc. Combust. Inst. 34 (1) (2013) 289-296.